Comparative morphoanatomy and transcriptomic analyses reveal key factors controlling floral trichome development in *Aristolochia* (Aristolochiaceae)

Harold Suárez-Baron[1,2], Juan F. Alzate[3], Barbara A. Ambrose[4], Soraya Pelaz[5,6], Favio González[7] and Natalia Pabón-Mora[2*]

[1]Department of Natural Sciences and Mathematics, Pontificia Universidad Javeriana Cali, Cali, Colombia.

[2]Instituto de Biología, Universidad de Antioquia, Medellín, Colombia.

[3]Centro Nacional de Secuenciación Genómica (CNSG), Sede de Investigación Universitaria, Facultad de Medicina, Universidad de Antioquia, Medellín, Colombia.

[4]The New York Botanical Garden, Bronx, NY, USA.

[5] Centre for Research in Agricultural Genomics, CSIC-IRTA-UAB-UB, Campus UAB, Bellaterra, Barcelona, Spain.

[6] ICREA (Institució Catalana de Recerca i Estudis Avançats), Barcelona, Spain.

[7]Universidad Nacional de Colombia, Facultad de Ciencias, Instituto de Ciencias Naturales, Bogotá.

[*]: corresponding author

harold.suarez@javerianacali.edu.co; jfernando.alzate@udea.edu.co; bambrose@nybg.org; soraya.pelaz@cragenomica.es; fagonzalezg@unal.edu.co; lucia.pabon@udea.edu.co.

Highlight

Comprehensive characterization of epidermal patterning and specialized perianth trichome development in dutchman´s pipe (*Aristolochia*) flowers, followed by the identification of candidate genes for multicellular trichome patterning in distantly related angiosperms.

Abstract

Trichomes are specialized epidermal cells in the aerial plant parts. Trichome development proceeds in three stages, determination of cell fate, specification, and morphogenesis. Most genes responsible for these processes have been identified in the unicellular branched leaf trichomes from the model *Arabidopsis thaliana*. Less is known about the molecular basis of multicellular trichome formation across flowering plants, especially those formed in floral organs of early diverging angiosperms. Here, we aim to identify the genetic regulatory network (GRN) underlying multicellular trichome development in the kettle-shaped trap flowers of *Aristolochia* (Aristolochiaceae). We selected two taxa for comparison, *A. fimbriata*, with trichomes inside the perianth, which play critical roles in pollination, and *A. macrophylla,* lacking specialized trichomes in the perianth. A detailed morphoanatomical characterization of floral epidermis is presented for the two species. Transcriptomic profiling at two different developmental stages in the different perianth portions (limb, tube, and utricle) of the two species is compared here. We present a comprehensive expression map for positive regulators and repressors of trichome development, as well as cell cycle regulators. Our data point to extensive modifications in gene composition, expression, and putative roles in all functional categories when compared to model species. We also record novel differentially expressed genes (DEGs) linked to epidermis patterning and trichome development. This work allows us to propose the first hypothetical genetic regulatory network (GRN) underlying floral multicellular trichome development in *Aristolochia* and pinpoints key factors responsible for the presence and specialization of floral trichomes in phylogenetically distant species of the genus.

Key words

Cell fate, *Aristolochia,* epidermis development, multicellular floral trichomes, perianth, RNA-seq

Introduction

Precise control of gene expression is crucial for proper cell differentiation and function, allowing the development of complex multicellular organisms (Babtie *et al*., 2019). Genetic regulatory networks (GRNs) are determined, in part, by the co-expression of transcriptional regulatory genes, which play a key role in defining the identity of organs, tissues, and cell types (Davidson and Peter, 2015). The study of GRNs in plants has predominantly focused on organ identity, leaving a gap in our understanding of cell fate regulation. This intricate process demands precise control over cell proliferation, differentiation, intercellular communication, and morphogenesis (An *et al*., 2011). In general, how plant cell-type-specific GRNs are established during development remains poorly understood, particularly in unraveling the mechanism by which neighboring cells acquire differential fates within developing tissues. Addressing this fundamental question will shed light on a wide range of developmental processes in plants.

Trichomes are highly differentiated epidermal cells present mainly on the aerial plant organs, acting as micro-morphological structures often correlated to environmental conditions (Pattanaik *et al*., 2014; Ioannidi *et al*., 2016). Thus, trichomes serve as an ideal model for studying GRNs controlling cell fate determination and morphogenesis, and cell cycle control (Hülskamp, 2004; Yang and Ye, 2013). Trichomes serve various functions, encompassing the regulation of transpiration, temperature, and light reflectance, and protect leaf tissues against UV radiation. They can also deter insect predation or act as mechano-sensory switches to promote toxin synthesis during herbivory (Levin, 1973; Wagner, 1991; Karabourniotis *et al*., 1992; Wagner *et al*., 2004; Glover *et al*., 2004; Pattanaik *et al*., 2014; El Ottra *et al*., 2013; Tan *et al*., 2016; Zhou *et al*., 2016; Liu *et al*., 2017). Noticeably, multicellular trichomes play critical roles in the specialized trapping system of the *Aristolochia* flower, where conical trichomes temporarily trap insects inside the perianth, while secretory trichomes produce substances that can feed them during pollination (Dafni, 1984; Pabón-Mora *et al*., 2015; Erbar *et al*., 2016; Suárez-Baron *et al*., 2019).

The molecular basis of unicellular trichome formation is well known in *Arabidopsis,* where it has been described primarily as an activator-inhibitor complex with positive and negative regulators. The upstream, positive regulators controlling trichome cell fate are GLABRA1 (GL1), an *R2R3 MYB* homolog (Oppenheimer

et al., 1991), that acts partially redundant with its paralog MYB23 during trichome initiation (Kirik *et al*., 2005); the bHLH proteins GLABRA3 (GL3) (Payne *et al*., 2000) and its homolog ENHANCER OF GL3 (EGL3) (Bernhardt *et al*., 2003; 2005; Zhang *et al*., 2003); and the WD-40 repeat-containing protein TRANSPARENT TESTA GLABRA1 (TTG1) (Walker *et al*., 1999). These proteins interact forming the MBW (MYB-bHLH-WD40) activation complex (Koorneef *et al*., 1982; Hülskamp *et al*., 1994, Payne *et al*., 2000; Bernhardt *et al*., 2005). This complex, in turn, activates the expression of *GLABRA2* (*GL2*), which encodes a homeodomain-leucine zipper (HD ZIP) protein that promotes trichome formation (Rerie *et al*., 1994). Negative regulators include TRIPTYCHON (TRY) and CAPRICE (CPC), which were initially identified by mutants showing trichome clusters (Schellmann *et al*., 2002; Digiuni *et al*., 2008). Furthermore, additional homologs such as *ENHANCER OF TRY AND CPC1* (*ETC1*) and *ETC2* (Kirik *et al*., 2004a; 2004b), *TRICHOMELESS1* (*TCL*) (Wang *et al*., 2007), and *CAPRICE-like MYB3* (*CPL3*) were discovered to act in a partially redundant manner. Other genes function as key factors in cell wall components providing strong light-reflecting properties to *Arabidopsis* trichomes; these include members of the *GLASSY HAIR* (*GLH*) genes and the closely related *NOECK* (*NOK*) and *TRICHOME BIREFRINGENCE* (*TBR*) (Sou et al., 2013).

In contrast to the well-documented molecular basis of unicellular trichome development, our understanding of the regulatory mechanisms and key factors involved in multicellular trichomes is still limited. Although several positive regulators and pathways have been identified, there is a significant gap regarding the molecular processes underlying multicellular trichome development. Available data on multicellular trichome development are primarily restricted to a few eudicots such as *Nicotiana* (Solanaceae), where the MBW complex has been reported (Yang *et al*., 2015), and the MYB transcription factor MIXTA has been identified as an inducer of multicellular trichomes (Payne *et al*., 1999; Perez-Rodriguez *et al*., 2005). In *N. tabacum* and *Solanum lycopersicum* the initiation of multicellular glandular trichomes has been associated with class IV HD-ZIP homologs (Yang *et al*., 2011; Yang *et al*., 2015). In addition, the induction of cell divisions during trichome early development in *S. lycopersicum* requires the activation of cell cycle regulators like cyclins, which modulate the shift between mitosis and endoreduplication (Chalvin et al., 2020; Yang et al., 2011). Other studies have been carried out in *Cucumis sativus* (Cucurbitaceae), where genes such as *CsGL3, CsGL2, CsMYB6*, and *CsWIN1* have been proposed as key factors for multicellular trichome initiation (Liu *et al*., 2016; Wang *et al*., 2021; Han *et al.,* 2022). Furthermore, in *Artemisia annua* (Asteraceae), newly characterized positive trichome regulators include

the R2R3 transcription factor, AaMYB17(Qin *et al*., 2021), while negative regulators include the *cyclin trichome less* (*AaCycTL*) gene(Dong *et al*., 2021).

As trichome development integrates external signals and endogenous developmental programs, phytohormones have been identified as critical players in cell fate specificity of the epidermis. In *Arabidopsis*, cytokinins (CKs), gibberellins (GAs), and jasmonic acid (JA) stimulate trichome initiation (Perazza et al., 1998; Traw and Bergelson, 2003; Yoshida *et al*., 2009; Qi *et al*., 2011). Phytohormones can also regulate the MBW complexes by activating cell fate determining transcription factors. These include the ZINC FINGER PROTEIN 5 (ZFP5), ZFP6, ZFP8, GLABROUS INFLORESCENCE STEMS (GIS), GIS2, TEMPRANILLO 1 (TEM1), and TEM2 (Gan *et al*., 2006; Gan *et al*., 2007; An *et al*., 2011; Zhou *et al*., 2013; Matías-Hernández *et al*., 2016).

Here, we aim to identify the GRN underlying multicellular trichome development in the sepal-derived perianth of *Aristolochia*. We present a detailed atlas of the inner perianth epidermis in two contrasting species: *Aristolochia fimbriata* and *Aristolochia macrophylla* (Figs. 1-4). The former is a member of the monophyletic subgenus *Aristolochia*, characterized, among other traits, by the presence of abundant and specialized multicellular trichomes inside of the flowers. In contrast, the latter is a member of the monophyletic subgenus *Siphisia*, whose flowers lack trichomes internally, at least in the limb and the tube (Figs. 1-4). We map the expression of all homologs previously identified in model species putatively involved in trichome determination cell fate, patterning, and morphogenesis in the two species, at two different developmental time points. We also identify differentially expressed genes (DEGs) between the three portions of the perianth (namely, the limb, the tube, and the utricle) of *A. fimbriata* and *A. macrophylla*. This is the first comprehensive study of floral epidermis development in early diverging angiosperms aiming to assess the hypothetical genetic regulatory network responsible for floral multicellular trichome development. These analyses serve as a reference for target genes involved in specialized perianth trichome development in non-model plant species.

Materials and methods

Plant Material

Flowers of *Aristolochia fimbriata* and *A. macrophylla* were collected (Figs. 2, 3). The *A. fimbriata* floral buds were obtained from the living collections at the New York Botanical Garden (NYBG, Bronx, NY) and the Universidad de Antioquia (Medellín, Colombia) (Plant ID: N. Pabón-Mora 242); the *A. macrophylla* flowers were collected at the Arnold Arboretum, Harvard University (Roslindale, MA) (Plant ID: 1112-88*A). In our experiments, *A. fimbriata* serves as a reference system to study the genetic basis for trichomes found in the inner floral epidermis (Suárez-Baron *et al*., 2021; Figs. 2, 4B, D, F). Conversely, the partially glabrous *A. macrophylla* serves for comparison as it lacks trichomes in the inner epidermis of the tube and the limb (Figs. 3, 4I, J, L). Two developmental stages were collected for each species (S6 and S9). Flowers were photographed using a Nikon D5000 and then fixed in 70% ethanol for morpho-anatomical evaluation. Other floral buds from the same plants were used for the molecular analyses.

Light Microscopy

Detailed morphoanatomy of the floral perianth in *Aristolochia fimbriata* and *A. macrophylla* was documented to identify stages of trichome development. Floral buds of the two species at S6 and S9 were prepared using a standard series of ethanol and HistoChoice® with a final step of tissue embedding in paraplast X-tra. Flowers were sectioned using an 820 Spencer microtome at 12 µm. Sections were stained in safranin and astra blue, mounted in Permount, and examined and photographed using a Zeiss – Primo Star Compound Microscope equipped with an Axiocam ERc 5s –Zeiss digital camera with Zen 2.3 Lite software.

Scanning Electron Microscopy

Three-dimensional patterning of the inner and the outer perianth epidermis was documented through conventional SEM microscopy. Sagittal sections of collected flowers in 70% ethanol were dehydrated in a series of 90%, 100% ethanol, 50:50% ethanol-acetone, and 100% acetone, critical point-dried using a Samdri 790 CPD (Rockville, MD, USA), and coated with gold and palladium using a Hummer 6.2 (Anatech, Springfield, VA, USA). Both, the inner and the outer epidermis were photographed at 10 kV on a Jeol JSM-5410 LV scanning electron microscope.

Transcriptomic analyses

With the goal of assessing gene expression in the three portions of the perianth at two different developmental stages in the trichome bearing *Aristolochia fimbriata*, eighteen *de novo* transcriptomes were generated. Each transcriptome was obtained from three independent biological replicates of the dissected portions of the perianth, namely, the utricle, the tube, and the limb. Two different developmental stages were compared, namely S6 and S9 (Figs. 1, 2A, B). For comparison, six *de novo* transcriptomes from *A. macrophylla* were obtained from the utricle, the tube, and the limb at S6 and S9 (Fig. 3A, B). Total RNA was extracted using TRIZOL reagent (Invitrogen; Carlsbad, CA, United States). The RNA-seq experiment was conducted using the Truseq stranded mRNA library construction kit (Illumina; San Diego, CA, United States) and sequenced on a NovaSeq 6000 system reading 100 bp, paired-end reads. Read cleaning was performed with a homebrew program with a quality threshold of Q30 at both ends and only keeping those longer than 70 bases after quality trimming. Contig assembly was computed using the Trinity package following default settings. Transcriptome assembly was performed for each sample (i.e., perianth region), at S6 and S9 (Supplementary Tables S1 – S2). In addition, a combined global transcriptome for each species was assembled as a reference. The metrics are as follows. For *A. fimbriata*: total assembled bases: 150608833 bp; the total number of contigs (> 101 bp): 118941; average contig length: 719 bp; contig N50: 14432 sequences ≧ 1823 bp; contig N75: 31828 sequences ≧ 746 bp; contig GC%: 42.71%. For *A. macrophylla*: total assembled bases: 164714213 bp; the total number of contigs (> 101 bp): 126783; average contig length: 1299 bp; contig N50: 25812 sequences ≧ 2127 bp; contig N75: 50215 sequences ≧ 1295 bp; contig GC%: 43.25%.

Mapping, gene isolation, expression by RNA-seq, and functional annotation

First, a directed search of trichome-related genes reported from unicellular trichomes in the model species *Arabidopsis thaliana* (https://www.arabidopsis.org/) and multicellular trichomes in *Cucumis sativa* was carried out in order to identify possible homologs in the *A. fimbriata* transcriptome. This step began with a search for all homologs using as queries the best hits from *Arabidopsis*. BLAST searches resulted in hits with an *e-value* of 1 x 10^{-30} for each query, where contigs were manually edited to find their ORF, and remove the 5' and 3' UTRs. The resulting contigs were blasted again in NCBI and TAIR, and only those with annotated hits were retained (Supplementary Table S3). To estimate the relative abundance of the assembled contigs, cleaned reads were mapped against the *de novo* assembled dataset implementing the algorithm Kallisto v.0.46.0 with default settings (https://pachterlab.github.io/kallisto/). Kallisto quantifies transcript expression normalizing the relative abundance of each contig/transcript using the transcript per million (TPMs) metrics (Bray *et al*., 2016). The heat maps were constructed using the Shinyheatmap program (https://github.com/Bohdan-Khomtchouk/shinyheatmap), and using the hierarchical clustering option to facilitate the visualization of DEGs' clusters (Khomtchouk *et al*., 2017).

Next, we performed an undirected search for new factors possibly involved in the epidermal differentiation and elaboration between the limb, tube and utricle at S6 versus S9. Three comparisons were performed to find differentially expressed genes (DEGs) among the three-perianth portions at two different developmental stages (Fig. 7). DEGs were identified as those with a False Discovery Rate (FDR) ≤ 0.05, a *p-value* ≤ 0.05, and a fold change > 5 or < -5 (Supplementary Table S4). First, we identified the top 60 DEGs in each of the floral parts for the two developmental stages in each species (Supplementary Tables S5 – S6). In turn the TPMs from the limb S6 *versus* limb S9, tube S6 *versus* tube S9, and utricle S6 *versus* utricle S9, were used to construct the heatmaps for *A. fimbriata* (Fig. 8; Supplementary Fig. S2) and for *A. macrophylla* (Supplementary Figs. S1-S2). In order to assess the represented functional categories in our comparative transcriptomic analyses, the identified DEGs were analyzed using a gene ontology (GO) enrichment through Blast2GO (https://www.blast2go.com/) (Supplementary Tables S7 – S8, Supplementary Fig. S3 – S4).

Genetic regulatory network (GRN) reconstruction

Next, in order to assess how the different functional categories and DEGs involved in epidermis development are related, we reconstructed a putative genetic regulatory network controlling trichome development. A total of forty-seven DEGs were chosen for their direct contribution to trichome initiation, differentiation, and morphogenesis. These include transcription factors, genes related to hormonal responses, and key cytoskeleton organization and cell cycle regulators. These were first identified by a thorough literature review. Some have also been confirmed as trichome related genes based on their recorded spatio-temporal expression patterns assessed by *in situ* hybridization (Suárez-Baron *et al*., 2021) or by having significant differential expression between S6 and S9 (Figs. 5, 7). Then, for the *in silico* prediction of protein-protein interactions the contigs were permanently translated and uploaded in STRING (version 11.0) (Szklarczyk *et al*., 2017). Because the *Aristolochia fimbriata* genome is not available through STRING, we tried to use the interactions available for the early diverging *Amborella trichopoda*; however, STRING does not have enough available information for *A. trichopoda*. Thus, we decided to use *Arabidopsis thaliana* to graph putative interactions between the selected proteins. Nodes were grouped together with their neighbors based on their clustering coefficient (Supplementary Figs. S5-S6, Supplementary Table S9).

Quantitative Real-Time PCR validation

To validate the differential expression found in the RNA-seq analyses we used quantitative Real Time-PCR (qRT-PCR) (Supplementary Fig. S7-S9). Assays were performed in freshly collected samples of *Aristolochia fimbriata.* Each sample is the result of three independent biological replicates pulled together. The same floral dissections and protocols for RNA extraction and cDNA synthesis described above, were used. The qRT-PCR master mix was prepared using Maxima SYBR-Green/ROX qPCR Master Mix K0222 (Waltham, MA, United States). The resulting cDNA was diluted 1:3. The PCR products were amplified using locus-specific primers designed by introducing selected regions of the target genes into http://www.genscript.com/ssl/bin/app/primer (Supplementary Table S10). The thermal cycling regime consisted of one initial step at 95ºC for 5 s, 54ºC for 5 s, and finally 72ºC for 20 s in a qTOWER3 G Real-Time Thermocycler (Analytik Jena, Jena, Germany). *Glyceraldehyde 3-phosphate dehydrogenase* (*AfimGAPDH*), *Actin7* (*AfimACT7*), *Ubiquitin* (*AfimUBQ*), and *Elongation factor 1α* (*AfimEF1α*) homologs from *A. fimbriata*

were isolated from the transcriptome and were tested as putative endogenous controls. *AfimACT7* and *AfimUBQ* were selected as the endogenous controls for gene target quantification. Endogenous controls were used in an independent manner or as the geometric mean between the two without large differences in the results. The levels of *LATERAL ORGAN BOUNDARIES* (*AfimLOB*), *SUPERMAN* (*AfimSUP*), *Transcription factor MYB117* (*AfimMYB117*), *HOTHEAD* (*AfimHTH*), *HISTONE 4* (*AfimH4*), and *SPEECHLESS* (*AfimSPCH*) were assessed. Transcript levels were calculated by implementing the $2^{-\Delta\Delta Ct}$ method (Livak and Schmittgen, 2001).

Results

Perianth morphoanatomy of *Aristolochia fimbriata*

The *Aristolochia fimbriata* perianth differentiates into a proximal inflated utricle, followed by a narrow tube that ends in an expanded limb with marginal extensions, known as the fimbriae. These are multicellular, vascularized processes with osmophores (specialized structures that produce and emit scents) and hooked trichomes (Figs. 1, 2B-G, 4A- H). In *A. fimbriata*, the most obvious change between S6 and S9 besides an increase from ca. 1 cm to ca. 4.5 cm in length, is the green-to-purple shift of the inner epidermis of the limb and tube (Figs. 1, 2A-C, 3A, H). In the S6 floral developmental stage, trichomes are barely seen by the naked eye, as they are beginning to differentiate (Figs. 1A-C, 2A, D, E, H, I, L, M). In fact, this is also the smallest stage for flower development that can be dissected in the three perianth portions under a stereoscope, hence the earliest one we could sample for RNA extraction in the absence of laser microdissection tools. In *A. fimbriata*, a comprehensive description of the developmental stages of the floral trichomes was made based on cell division and growth patterns (Fig. 1). Trichome development initiates with a single epidermal cell undergoing an additional mitotic division and progressively proceeds through subsequent cell divisions, facilitating the elongation and growth of the trichome perpendicular to the epidermal layer (Fig. 1A-1C). At S6 floral developmental stage, trichomes are found in developmental stage three (S3), which means they have initiated, but have not achieved their final morphogenesis. The final developmental stage for trichome morphogenesis (trichome stage S6), corresponds to *A. fimbriata* flowers of ca. 4.5 cm, at floral developmental stage S9, which are purple in the inner surface of the limb and the tube (Fig. 1A-C, 2B, F, G, J, K, N, O). Concomitantly, there are changes in the ornamentation of the inner epidermis in each perianth

portion, which is covered by distinct types of multicellular trichomes. The limb bears three-celled hooked trichomes of ca. 80 µm (Figs. 1A, 2D-G, 4B). The tube has conical secretory trichomes of ca. 80 -120 µm, averaging 24 cells including the narrow basal cell (Figs. 1B, 2H-K, 4D). Finally, the utricle has filamentous, secretory trichomes of ca. 150 -200 µm and averaging 28 cylindrical cells, interspersed by osmophores and nectarioles (specialized nectaries present on the epidermal tissue inside floral organs) (Figs. 1C, 2L-O, 4F). By sampling S6 and S9 floral developmental stages we can compare two different developmental stages during trichome differentiation (S3 and S6 respectively) with little variation in the mesophyll, formed by tightly packed parenchymatic cells (Figs. 1A-C, 2D-O). The outer green to yellow epidermis lacks trichomes, is homogeneously formed by flat cells with interspersed stomata and does not undergo major changes during development (Fig. 2A, B, D-F, H-J, L-N, 4C, E, G, H).

Perianth morphoanatomy of *Aristolochia macrophylla*

The *Aristolochia macrophylla* perianth increases from ca. 1 cm to ca. 4.5 cm in length between S6 and S9 (Figs. 3A-C, 4I-P). The stage S6 in *A. macrophylla* is characterized by the presence of scattered multicellular trichomes found in the outer epidermis protecting the floral bud (Fig. 3A, D, E, H, I, L, M). Stage 9 (S9) corresponds to the preanthetic flowers (Fig. 2B, 3B). However, S9 in *A. macrophylla* is not significantly different from S6 as only a small number of multicellular trichomes can be observed in the outer epidermis (Fig. 4K, M). However, the inner epidermis of the tube remains glabrous (Fig. 4L). Only multicellular filamentous trichomes are scattered in the inner and outer epidermal portions of the utricle (Figs. 4N-O). Perianth color shifts from primarily green throughout at S6 to a yellowish limb, a reddish tube and a purple utricle at S9 (Figs. 3A-C, 4I, P). In contrast to *A. fimbriata*, the *A. macrophylla* perianth lacks trichomes in the inner epidermis of the limb and the tube, and the epidermis exhibits papillae covered by a cuticle interspersed by stomata (Figs. 3D-K, 4J, L). Unlike the other two floral portions, the inner epidermis of the utricle has multicellular filamentous trichomes (Figs. 3L-O, 4N). The *A. macrophylla* mesophyll is less densely packed than that of *A. fimbriata*, and has large intercellular spaces, particularly towards the outer surface (Fig. 3D-O). The inner utricle epidermis has scattered stomata, and the multicellular filamentous trichomes are mostly located closer to the distal portion, and decrease on the perianth base around the gynostemium (i.e., the complex structure formed by the congenital fusion of stamens and stigmas) (Fig. 4N). Finally, the outer greenish epidermis has scattered multicellular hooked and conical trichomes (Fig. 4K, M, O).

Targeted search and expression of epidermal and trichome-related genes in *Aristolochia fimbriata*

Our main goal was to identify the expression of all genes putatively related to trichome differentiation, and morphogenesis in *A. fimbriata.* We performed a targeted search using as queries 124 trichome-related genes previously identified. Regardless of the species from which genes were identified and described, we started the search using the *Arabidopsis thaliana* homologs. Only 82 were found unambiguously as single copy genes in the *A. fimbriata* global floral transcriptome (Supplementary Table S6). The expression level of these homologs was evaluated in the limb, tube, and utricle at S6 and S9 in *A. fimbriata*. We focused primarily on the genes found up-regulated in S6 in the three evaluated perianth portions, with the premise that trichome initiation cues were still present and early morphogenesis genes are expressed actively at this stage (Fig. 5). These genes include several members of the MBW trichome initiation complex including the closest homolog of *GLABRA1, AfimMYB23*, and the downstream key gene for trichome morphogenesis *GLABRA2* homolog, *AfimGL2,* as well as the cytokinin responsive trichome activating *Zinc finger protein-6* and *8* (*AfimZFP8* and *AfimZFP6*).

We found a higher expression at S6 (compared to S9) of the following genes: the *Guanine nucleotide exchange factor SPIKE 1* (*AfimSPK1*), involved in trichome shape; several cell cycle regulators, cell proliferation and microtubule organization related genes including *Chromatin assembly factor 1 subunit FAS1* (*AfimFAS1*), *Histone chaperone ASF1A* (*AfimASF1A*), *transcription factor E2FB* (*AfimE2FA*-like), *actin-related protein C5A* (*AfimARPC5A*), *Kinesin-like protein KIN-12B* (*AfimKIN-12B*), and *HISTONE4* (*AfimHIS4*). We also detected several highly specialized genes with roles in cuticle integrity (The *HOTHEAD* homolog *AfimHTH*), wax biosynthesis (The *ECERIFERUM1* factor *AfimCER1-like*), as well as Jasmonate glandular trichome based defenses (the *Coronatine-insensitive protein 1 AfimCOI1*). Interestingly, the key trichome negative regulator *MYB6* (*AfimMYB6*) is upregulated at the earliest stage examined (S6).

Other transcription factors known to be critical in trichome initiation, including *AfimMYB106-like* (*NOK, MIXTA*-like R2R3), *AfimWIN1* (*WAX INDUCER 1*), *AfimRAV1*-like (*ETHYLENE RESPONSE DNA BINDING FACTOR*), and the *MYB-like transcription factor ETC3* (*AfimETC3*), are also upregulated in S6 compared to S9, but only detected with significant differential expression in the limb and the tube (Fig. 5). Upregulated

genes in the limb and the utricle at S6 include the *Retinoblastoma-related protein 1* (*AfimRBR1*), *Histone-binding protein MSI1* (*AfimMSI1*), *Chromatin assembly factor 1 subunit FAS2* (*AfimFAS2*), and *Protein WAVE-DAMPENED2* (*AfimWVD2-like3*). Finally, one gene was found upregulated only in the tube and utricle at S6, the *CDPK-related kinase 5* (*AfimCDPK5*-like).

Differentially expressed genes (DEGs) in the *Aristolochia fimbriata* perianth portions

With the goal of identifying novel (not previously targeted) genes putatively important for epidermal patterning, we recorded the differentially expressed genes (DEGs) between S6 and S9 in the three perianth portions (limb, tube, and utricle) of *A. fimbriata*. This analysis allowed us to find a total of 6679 DEGs between S6 and S9, as follows: 2093 in the limb, 1961 in the tube, and 2625 in the utricle (Fig. 6). In order to identify putative gene candidates contributing to the changes observed between S6 and S9, we decided to concentrate first on the top 60 DEGs, including the top 30 up- and down-regulated DEGs for each floral region (Fig. 7, Supplementary Table S6). Gene Ontology (GO) analyses allowed us to assign 55% of the DEGs in the *A. fimbriata* perianth to the following molecular functions: ATP-binding, metal ion and zinc ion binding, transferase activity, oxidoreductase activity, DNA binding and protein kinase activity. Most of the DEGs could be identified as integral components of membrane (35%), nucleus (13%) or cytoplasm (8%). The majority of the DEGs (72%) have not been assigned to a particular biological process; however, 32% of those with GO categories are linked to oxidation-reduction process, regulation of transcription, and protein phosphorylation. Other less represented categories but perhaps more important for epidermis development include the following biological processes: microtubule-based movement, microtubule depolymerization, cell wall organization and biogenesis, and trichome morphogenesis (Supplementary Figure S3).

Our comparisons identified four up-regulated genes in all perianth portions at S6, namely, *Glycine protein 5* (*AfimGRP5*), a *Vestitone reductase-like* (*AfimVERE*), an *Auxin Response factor 5* (*AfimARF5*), and the transcription factor *SPEECHLESS*-like (*AfimSPCH*). A single common upregulated gene at S9 in all three perianth portions corresponds to a Benzyl alcohol O-benzoyltransferase (*AfimHSR201*). A close inspection of the top 60 *A. fimbriata* perianth DEGs allowed us to identify that several homologs previously linked to epidermis development were upregulated exclusively at S6. For instance, the *HOTHEAD*-like gene

(*AfimHTH*) is restricted to the limb. Conversely, the following transcription factors were found in the limb and the tube: an *ECERIFERUM 1*-like (*AfimCER1*-like) gene; an *ASYMMETRIC LEAVES1* (*AfimAS1*) homolog; and the *Homeobox-leucine zipper protein ANTHOCYANINLESS 2* (*AfimANL2*). Epidermis-related genes were not found among the DEGs at S9 (Fig. 7).

Other factors directly linked to cell division and microtubule organization in epidermal cells exhibit the same early activation exclusive to S6. These are: *Kinesin-like 13-A* (*AfimKIN13-A*) and *12-F* (*AfimKIN12-F*); a *Phragmoplast orienting kinesin 2* (*AfimPOK2*); *CYCLIN A2:4* (*AfimCYCA2:4*); a tubulin component *TUBA1* (*AfimTUBA1*); and the *Growth-regulating factor 1* (*AfimGRF1*) (Fig. 7). Finally, several structural and metabolic genes were also found to be up-regulated at S6, including: a *Nitronate monoxigenase*-like (*AfimNMO*) enzyme in the limb and the tube; an *Aspartate aminotransferase* (*AfimASP*) and the *Sedoheptulose-1,7-biphosphate* (*AfimSED1-7*) in the limb; a *GDSL esterase/lipase* (*AfimGDSL*) in the tube; and the *Cytochrome P45078A11* (*AfimP45078A11*) and the *WUSCHEL-related homeobox 2* (*AfimWUS2*) genes in the utricle.

Differentially expressed genes (DEGs) in the *Aristolochia macrophylla* perianth portions

Using the same strategy, we found a total of 2550 DEGs in *A. macrophylla* between S6 and S9, specifically 971 in the limb, 714 in the tube, and 865 in the utricle (Fig. 6). Gene ontology (GO) analyses of the *A. macrophylla* dataset is largely overlapping to that of *A. fimbriata* in molecular function, cellular components, and biological processes (Supplementary Fig. S4). However, many of the epidermis-related putative processes, including microtubule depolymerization, pattern specification, cell wall organization and biogenesis, and trichome morphogenesis, are no longer present in this dataset.

In the *Aristolochia macrophylla* dataset, the top 60 DEGs were also targeted (Supplementary Fig. S1). Considering that a large number of factors can control DEGs, we decided to find key factors in the dataset that could be linked to differences in perianth epidermal patterning and especially trichome development in comparison with *A. fimbriata*. The DEG dataset in *A. macrophylla* identified five upregulated genes in all perianth portions at S9. These include the *protein TIFY 5A* (*AmaTIFY5A*), a fatty acid amide hydrolase-like

(*AmaFAAH*), a *Xyloglucan endotransglucosylase/hydrolase protein* (*AmaXTH30*), a *Mini zinc finger protein 2* (*AmaZFP2*), and the *NAC domain-containing protein* (*AmaNAC100*). A close inspection of the top 60 *A. macrophylla* perianth DEGs allowed us to identify that several homologs previously linked to epidermis patterning and cell division control were upregulated exclusively at S6. These are: a *CYCLIN B2-4* homolog (*AmaCYCB2-4*), a *Kinesin-like protein KIN-5A* (*AmaKIN-5A*), and the Homeobox-leucine zipper homolog *ANTHOCYANINLESS 2* (*AmaANL2*), all of them active in the limb. Additionally, the *TOO MANY MOUTHS* (*AmaTMM*) gene, the *EPIDERMAL PATTERNING FACTOR-like protein 9* (*AmaEFLP9*); the *Phragmoplast orienting kinesin 2* (*AmaPOK2*), the key trichome inhibiting factor *TRYPTYCHON* (*AmaTRY*), and the *Zinc finger proteins-6 and -8* (*AmaZFP6* and *AmaZFP8*) were found upregulated at S6 in the tube and the utricle.

Aristolochia fimbriata transcriptomic differential expression data validation by RT-qPCR

To assess the reproducibility of the differentially expressed genes (DEGs) identified by transcriptomic analyses, we conducted qRT-PCR experiments using new biological replicates, specifically, RNA samples of the limb, the tube, and the utricle from *A. fimbriata* at S6 and S9. A total of six genes were randomly selected for validation. All qRT-PCR results mirrored the expression patterns of the RNA-seq data (Supplementary Fig. S7-S9).

Epidermal genetic regulatory network (GRN) reconstruction in the *Aristolochia* perianth

A comprehensive genetic regulatory network (GRN) using the trichome related DEGs of *A. fimbriata* was constructed using STRING (Supplementary Fig. S5-S6). This interaction network consisted of seventy-four edges and forty nodes, each node showing a specific epidermal-related protein homolog identified in *Aristolochia* (Supplementary Table S9). Thirty of these clustered proteins were selected from the differentially expressed genes found in this study. The remaining ten proteins correspond to genes for which patterns of expression were previously evaluated in *A. fimbriata* using *in situ* hybridization assays (Suarez-Baron *et al*., 2021). These genes fall into the following seven categories: (1) proteins that are associated with the MBW complex of trichome formation and its regulators, including some hormonal transduction proteins; (2) proteins associated with epidermal development and epicuticular wax

biosynthesis; (3) proteins involved in the control of cell cycle progression; (4) proteins related to the regulation of actin polymerization and control of cell morphogenesis via the modulation of cell polarity; (5) histone and chaperone proteins as components of the chromatin assembly; (6) kinesin proteins involved in the control of cell morphogenesis and cytoskeleton dynamics; and (7) proteins involved in stomatal development. Finally, using all the analyzed transcriptomic data and information about the expression patterns obtained from *in situ* hybridization experiments (Suarez-Baron *et al.*, 2021), we propose a hypothetical genetic regulatory network for multicellular floral trichome development in *Aristolochia* and the surrounding non-trichome cell fate specification (Fig. 8).

Discussion

Here, we have characterized the development of multicellular floral trichomes during flower development of *A. fimbriata* and have assessed the most important genetic players underlying their growth and morphogenesis. Within the inner epidermis of the limb, tube, and utricle, trichome development stage one (S1) represents the initiation of a trichome precursor cell, while stage six (S6) indicates a mature trichome (Fig. 1). The developmental process begins with a single epidermal cell division and progressively proceeds through subsequent cell divisions, facilitating trichome elongation and growth perpendicular to the epidermal layer (Fig. 1A-1C). The inner epidermis of the utricle is carpeted by multicellular, filamentous, secretory trichomes interspersed with osmophores. In contrast, three-celled hooked trichomes cover the inner epidermis of the limb, while multicellular conical trichomes are located the inner epidermis of the tube (Figs. 1A-1C, 4A-B, D, F). Our transcriptomic data comes from: trichome development stage S3 (floral developmental stage S6), that represents the earliest sampling possible, where trichomes have been formed but are not yet fully developed, and trichome development stage S6 (floral developmental stage S9), where trichome morphogenesis has been completed into different trichome shapes in the three perianth portions. The comparative transcriptomic analyses in *Aristolochia fimbriata* and *A. macrophylla,* enabled us to identify several DEGs associated with trichome maturation, in addition to transcription factors that can act as phytohormone integrators. We also assess the role of cell cycle regulators in floral trichomes. It is important to highlight that factors involved in strict trichome initiation or cell fate changes in the epidermis cannot be readily characterized in the stages chosen for *A. fimbriata.* However, expression data of trichome initiation genes obtained at S6 by RNAseq data coincides with spatio-temporal expression patterns during trichome initiation in previous studies (Suárez-Baron et al., 2021). This is suggestive of early

cell fate genes still being active during early trichome morphogenesis and therefore amenable to detection by transcriptomic analyses. Finally, we discuss newly identified genes correlated with the epidermal patterning in the three perianth portions of the two species. The data gathered helps to better understand cell fate in the *Aristolochia* floral epidermis.

Genes recruited for trichome cell fate determination, specialization, and morphogenesis in the flowers of *Aristolochia.*

By taking a candidate gene approach, we targeted previously identified genes in cell fate determination, cell polarity, cell expansion and cell morphogenesis reported during the formation of *Arabidopsis* unicellular trichomes (Schellmann and Hülskamp, 2005; Schnittger *et al*., 1999; Schellmann *et al*., 2002; Zhao *et al*., 2008; Balkunde *et al*., 2010), as well as *Cucumis sativus* multicellular trichomes (Zhao *et al*., 2015b; Liu *et al*., 2016). First, we targeted the positive regulators for trichome initiation, regardless of whether they had been identified in unicellular or multicellular trichomes (Folkers *et al*., 1997; Stracke *et al*., 2001; Jakoby *et al*., 2008; Noda *et al*., 1994; Baumann *et al*., 2007; Jaffé *et al*., 2007; Zhao *et al*., 2015b; Liu *et al*., 2016). These include the MBW complex members *GLABROUS1* (the R2R3-MYB partner), *GLABRA3*, *ENHANCER OF GLABRA3* (bHLH members), and *TRANSPARENT TESTA GLABRA1* (WD40 repeat homolog). In parallel, we also screened for *WIN1* and *MIXTA* homologs identified from *Cucumis.* We found homologs for all these genes in *Aristolochia* flowers. In addition to the previously targeted *GLABRA3* homolog *AfimGL3,* and the WD40 putative partner *AfimTTG1*, we were able to find *AfimMYB23,* the closest homolog for *GLABROUS1,* which so far remained elusive. This is interesting because *MYB23* is a close relative of *GL1* and *WEREWOLF* (WER), and the three R2R3-MYB genes are present in *Arabidopsis* (Stracke *et al*., 2001; Zimmermann *et al*., 2004; Kang *et al*., 2009). In fact, in *Arabidopsis MYB23* is partially redundant with *GL1* in the regulation of trichome initiation, extension, and branching (Kirik *et al*., 2005). We also identified the *WIN* homolog *AfimWIN1*, the *MYB6* homolog *AfimMYB6* and the *MIXTA* homolog *AfimMYB106-like.* The *MYB106* homologs, best known as *MIXTA*-like R2R3 MYB genes, are pivotal conserved transcription factors in trichome development and epidermal specializations across angiosperms. In *Arabidopsis*, the *MYB106* homologue (*NOECK*) controls trichome branching (Jakoby *et al*., 2008) and MIXTA-like genes regulate the growth of epidermal conical cells in the *Antirrhinum majus* and *Nicotiana tabacum* petals (Baumann *et al*., 2007; Jaffé *et al*., 2007). Also, homologs of *AtMYB106* have been reported in *Cucumis sativus* as candidates for trichome morphogenesis (Li *et al*., 2012; Yang *et al*., 2018). Likewise, in species of the non-core eudicot

genus *Thalictrum* (Ranunculaceae), the ortholog of *MIXTA*-like2 regulates cell shape in floral epidermis (Di Stilio *et al*., 2009). The most important downstream targets for trichome differentiation and branching are the positive regulators *GLABRA2*, and *HOMEODOMAIN GLABROUS2* (Marks and Esch, 1994; Rerie *et al*., 1994; Kamata *et al*., 2013). Their homologs were also found in *Aristolochia*, corresponding to *AfimGL2* and *AfimHDG2*.

Altogether, the dataset of positive regulators for trichome development in *Aristolochia* is more similar to that reported in *Cucumis* than that of *Arabidopsis*, pointing to common hubs for multicellular trichome development in distantly related angiosperms. Expression data, both from *in situ* hybridization and RNA-seq, excludes the participation of *AfimGL3* and *AfimTTG1* in trichome initiation (Suárez-Baron *et al*., 2021; Fig. 5). The two genes are poorly expressed at S6 and at least *AfimTTG1* was not detected during floral trichome initiation (Suárez-Baron *et al*., 2021; Fig. 5). All other homologs including *AfimMYB23*, *AfimMYB106-like, AfimWIN1*, and the target *AfimGL2*, are expressed at S6 (Fig. 5) and their spatial expression points to conserved roles in trichome initiation in *Aristolochia* flowers (Suárez-Baron *et al*., 2021). Thus, our model points to three putative partners: *AfimMYB23*, *AfimMYB106-like*, and *AfimWIN1*, that are turned on early in S6 and activate *AfimGL2* (Fig. 8). According to our data, higher levels of expression in the trichome constitutive cells of *AfimGL2* when compared to *AfimHDG2* suggests that the former is more important as a target of the complex than the later (Suárez-Baron *et al*., 2021; Figs. 5, 8).

Our study also confirm the participation of *RAV1-like* homologs in trichome development (Suárez-Baron *et al*., 2021; Fig. 5). In fact, our expression data of *AfimRAV1*-like points to a role in promoting multicellular trichome development, like that reported in *Cucumis sativus* (Zhao *et al*., 2015a), in contrast to the repressive function of trichome-related genes assigned to the *RAV* homologs *TEM1/2* in *Arabidopsis* (Matías-Hernández *et al*., 2016). The data gathered here also suggests that the positive trichome regulators, the C2H2 *ZINC FINGER PROTEINS (ZFP)*, specifically the *AfimZFP6* and *AfimZFP8,* may have similar roles to those reported in model species (Gan *et al*., 2007). Their early expression at S6 points to key functions in the interplay between trichome initiation genes (specifically *AfimGL2*) and different phytohormones, like gibberellins (GAs) and cytokinins (CKs) (Fig. 8).

Next, we targeted the negative trichome regulators. Our data do not rule out functions in negative regulation of trichome development for *AfimMYB6* (transcriptional repressor *MYB6*), and *AfimETC3* (*ENHANCER OF TRY AND CPC3*) genes expressed at S6, or *AfimTRY* (*TRIPTYCHON*) expressed at S9. The early activation of *AfimMYB6* and *AfimETC3* suggests that they control trichome distribution by inhibiting neighboring non-trichomatous cells from acquiring trichome cell fate, resembling their role in *Arabidopsis* and *Cucumis* (Yang *et al*., 2018) (Fig. 8).

We were also interested in identifying other factors related to trichome morphogenesis actively expressed at S6 in *Aristolochia* flowers. One gene, *AfimSPK1,* stood out as one of the few genes up-regulated in all three perianth portions at S6. Its homolog in *Arabidopsis, SPIKE* (*SPK1*), promotes polarized growth and controls proper trichome branching *via* actin-dependent cell morphogenesis (Qiu *et al*., 2002; Basu *et al*., 2008; Zhang *et al*., 2010). The high expression of *AfimSPK1* at S6 suggests that this factor controls trichome morphogenesis in all trichome types present in the three perianth portions of *A. fimbriata* flowers, and that it performs roles other than trichome branching, as all trichomes in *Aristolochia* flowers are unbranched.

Cytoskeleton organization and cell cycle genes putatively controlling trichome initiation and maturation in *Aristolochia* flowers

Epidermal morphogenesis relies on precisely coordinated cell division and cell expansion processes. During morphogenesis, trichomes develop from protodermal precursor cells. In *Arabidopsis,* whilst surrounding epidermal cells around the forming trichome continue to divide, the trichome cell skips the mitotic cycle to proceed to one or more endoreduplication cycles, characterized by DNA replication in the absence of nuclear and cellular divisions (Hülskamp *et al*., 1994). Endoreduplication can change cell polarity and concomitant growth direction (Schnittger and Hülskamp, 2002). In addition, cell cycle regulators have also been implicated in the maintenance of cell division during the development of multicellular glandular trichomes (Chalvin *et al*., 2020). A large number of putative cytoskeleton organization genes and cell cycle regulators were identified in our analyses, several of which are more active at S6 than at S9 (Fig. 5). Interestingly, and despite the fact that the earliest stage sampled already had undergone trichome initiation, some of these factors also appear among the top 60 DEGs in the trichome bearing *A. fimbriata* (Fig. 7). These include *AfimCYCA2-4*, *AfimCDKG-2*, *AfimE2FA*, and *AfimASF1A* in *A. fimbriata,* and

AmaCYCU2-1, *AmaCYCD3-1*, and *AmaCYCB2-4* in *A. macrophylla.* The A-type cyclins *CYCA2-3* and *CYCA2-4* in *Arabidopsis*, have been reported as key cell cycle-related genes regulating division and endoreduplication during trichome development. Similarly, D-type cyclins such as *CYCD3-1* can induce cell division in multicellular trichomes (Schnittger *et al*., 2002; Imai *et al*., 2006). Cyclin activation is also correlated with the expression of the transcription factor *E2FA* and the histone chaperone *ANTI-SILENCING FUNCTION1* (*ASF1A*) genes, at least in *A. fimbriata*. *AfimE2FA* and *AfimASF1A* are key components of the cyclin D-retinoblastoma-E2F pathway and histone-binding processes, respectively. Both play important roles in the control of cell cycle progression and cell proliferation during plant development (Sozzani *et al*., 2006; De Jager *et al*., 2009; Zhu *et al*., 2011). Their higher expression at early stages of floral development in *Aristolochia* strongly suggests that they are key cell-cycle control genes linked to the morphogenesis of multicellular trichomes. Notably, homologs of cell cycle inhibitor proteins, important in endoreduplication, like the *Arabidopsis SIAMESE* (*SIM*) gene, were not found in our transcriptomes.

Moreover, ten genes associated with cytoskeleton dynamics were also found to be upregulated at S6 in all three perianth portions of *Aristolochia*. Among these genes, there are six members of the kinesin superfamily of microtubule-based motor proteins, including the *AfimKIN-12F*, *AfimKIN-12B*, *AfimKIN-13A, AfimKIN-5A, AfimKIN-5D*, and *PHRAGMOPLAST ORIENTATING KINESIN 2* (*AfimPOK2*). Several *Arabidopsis* kinesins control microtubule organization, stability, and rearrangement (Ali and Yang, 2020). Some of them have been directly linked to trichome morphogenesis like the *Kinesin-13A* from cotton (*GhKinesin-13A*) and its homolog in *Arabidopsis KIN-13A* (Oppenheimer *et al*., 1997; Lu *et al*., 2005; Smith and Oppenheimer, 2005; Li *et al*., 2017).

In addition to the kinesins, other cytoskeleton organization and chromatin-related genes up-regulated at S6 include the Actin-related protein 2/3 complex subunit 5A (*AfimARPC5A*), the *Alpha-1-tubulin* (*AfimTUBA1*), the *WAVE-DAMPENED2* microtubule-associated protein MAP (*AfimWVD2-like3*), and the chromatin assembly factor 1 subunits *AfimFAS1* and *AfimFAS2*. In *Arabidopsis*, most of these genes have been linked with different aspects of cell morphogenesis (Kaya *et al*., 2001; Yuen *et al*., 2003; Perrin *et al*., 2007; Chen *et al*., 2008; Yanagisawa *et al*., 2015, 2018). Specifically, trichome expansion and shape complexity, as they depend on a microtubule cortical-arrangement perpendicular to the direction of trichome growth (Mathur *et al*., 1999; Mathur and Chua, 2000; Folkers *et al*., 2002; Szymanski, 2009; Sambade *et al*., 2014; Tian *et al*., 2015). Thus, our findings narrow down the candidate genes likely recruited

in microtubule and actin cytoskeleton organization that are most likely to control trichome morphogenesis in *Aristolochia* flowers.

Other perianth epidermal-related genes are differentially expressed during early developmental stages of the *Aristolochia* flower

Based on the findings that early stages of perianth development in *Aristolochia fimbriata* have higher expression of trichome initiation and morphogenesis genes compared to mature flowers, we carefully screened a total of 3489 upregulated genes at S6 in the three perianth portions of this species. Our goal was to identify transcription factors aiding in perianth epidermal patterning upstream, or concomitant to, trichome development. Additional factors found include a homolog of *ASYMMETRIC LEAVES1* (*AfimAS1*). The *Arabidopsis AS1* controls cell division and differentiation in leaves, as well as adaxial-abaxial leaf polarity (Sun *et al*., 2002; Byrne *et al*., 2000; Machida *et al*., 2015). *AfimAS1* stands out as a top candidate gene for maintaining ab-adaxial polarity in the *Aristolochia* perianth, perhaps even promoting different processes at the two perianth surfaces. Another gene upregulated at S6 is *AfimANL2*. In *Arabidopsis*, *ANTHOCYANINLESS 2* (a class IV HD-ZIP homolog) is involved in the accumulation of anthocyanin in epidermal and subepidermal leaf cells (Kubo *et al*., 1999), and has been recently linked to cuticle biosynthesis in tomato fruits (Nadakuduti et al., 2012) and the regulation of cell wall mechanical properties of *Arabidopsis* cotyledons (Mabuchi et al., 2016). Interestingly, HD-ZIP IV homologs are essential for the normal development of the epidermal tissue in *Arabidopsis* (Kamata *et al*., 2013). Thus, *AfimAN2* could be a candidate gene for proper development of the epidermis and anthocyanin accumulation in the *A. fimbriata* perianth. In the same manner, we identified a homolog of the *HOTHEAD* gene, *AfimHTH*. In *Arabidopsis, HTH* encodes an FAD-incorporating oxidoreductase, an important protein for limiting cellular interactions between contacting epidermal cells during floral development (Krolikowski *et al*., 2003), as well as cutin biosynthesis (Kurdyukov *et al*., 2006; Lü *et al*., 2009). Similar functions could be performed by *AfimHTH* in the *Aristolochia* perianth, pointing to a candidate factor in maintaining cell limits and presumably linked to the biosynthesis of cutin constituents. Finally, *AfimCER1-like*, a homolog of the *Arabidopsis ECERIFERUM1*-like gene, was also found upregulated at S6. This factor regulates different steps of the wax biosynthesis pathway in *Arabidopsis,* by the conversion of long-chain aldehydes to alkanes, promoting the wax very-long-chain alkane production and strengthen light-reflective properties of the cell wall (Bourdenx *et al*., 2011; Pascal *et al*., 2019).

The results presented here constitute the first putative floral trichome GRN in magnoliids and render: (1) a key reference for future evolutionary comparative studies of trichome development across angiosperms filling an important phylogenetic position outside of monocots and core eudicots, and (2) a testable hypothesis for how regulatory hubs can be formed between perianth development, epidermal patterning and trichome morphogenesis. For instance, it is possible that AfimHTH, AfimCER1, and AfimWIN1 closely interact as a hub between the trichome initiation and the cutin and wax biosynthetic pathways. In such a case, the waterproof barrier that constitutes the epidermal cuticle could be under the same genetic control in the *Aristolochia* perianth as it is in the *Arabidopsis* leaves. Altogether, our data shows that it is plausible to identify important hubs that link cell fate determination, cell cycle control, trichome morphogenesis and epidermal elaboration of the sepal-derived perianth of *Aristolochia,* by combining comparative transcriptomic data and *in silico* analysis of protein interactions.

Conclusions

Our findings constitute the first comprehensive study of floral epidermis development in early diverging angiosperms, and serve as a reference for targeting genes involved in specialized perianth trichome development in non-model plant species. Altogether, our results allow us to suggest for the first time a hypothetical genetic regulatory network for multicellular trichome development in the *Aristolochia* flower, including both the positive regulatory genes as well as the repressors of the genetic pathway. These results compare the core genetic network of multicellular trichome development in model species to that of flowers of *Aristolochia*. However, the predicted roles based on gene expression profiles and expression patterns will have to be confirmed through functional studies when available for this non-model species.

Acknowledgements

We thank to the New York Botanical Garden (NYBG), especially to Dr. Cecilia Zumajo-Cardona for assistance during lab work. We also thank William (Ned) Friedman, Kathryn Richardson, Michael S. Dosmann, and Faye Rosin at The Arnold Arboretum of Harvard University.

Author contributions

HS-B and NP-M conceived and designed the study; HS-B and NP-M performed the experiments; HS-B, NP-M, and JFA executed the bioinformatics analysis and analyzed data with support from all co-authors; HS-B, NP-M and FG designed the phylogenetically-based sampling within *Aristolochia*, and carried out the morphoanatomical studies; HS-B and NP-M led the writing of the manuscript with contributions from all the authors. All authors reviewed, edited, and approved the final version of the manuscript.

Conflicts of interest

The authors declare that they have no conflict of interest.

Funding

This work was supported by the Department of Science and Technology of Colombia -COLCIENCIAS and COLFUTURO [Conv. Doctorados Nacionales No. 727 de 2015] and the Estrategia de Sostenibilidad (2018-2019) awarded to the Grupo Evo-Devo en Plantas by the Universidad de Antioquia, Medellín, Colombia. Access to living collections, sequencing, and laboratory resources was possible thanks to *The Deland Award* (2018) and *The Jewett Prize* (2019) given by the Arnold Arboretum of Harvard University to HS-B and NP-M, respectively.

Data availability

The data are available upon request from the corresponding author (NP-M).

References

Ali I, Yang WC. 2020. The functions of kinesin and kinesin-related proteins in eukaryotes. *Cell Adhesion and Migration* 14, 139-152.

An L, Zhou Z, Yan A, Gan Y. 2011. Progress on trichome development regulated by phytohormone signaling. *Plant Signaling and Behavior* 6, 1959-1962.

Babtie AC, Stumpf MPH, Thorne T. 2019. Gene regulatory network inference. In: Voit, E. (ed.) Reference module in biomedical science. Elsevier. doi: 10.1016/B978-0-12-801238-3.11346-7

Balkunde R, Pesch M, Hülskamp M. 2010. Trichome patterning in *Arabidopsis thaliana*: from genetic to molecular models. *Current Topics in Developmental Biology* 91, 299-321.

Baumann K, Perez-Rodriguez M, Bradley D, Venail J, Bailey P, Jin H, *et al.* 2007. Control of cell and petal morphogenesis by *R2R3 MYB* transcription factors. *Development* 134, 1691-1701.

Basu D, Le J, Zakharova T, Mallery EL, Szymanski DB. 2008. A SPIKE1 signaling complex controls actin-dependent cell morphogenesis through the heteromeric WAVE and ARP2/3 complexes. *Proceedings of the National Academy of Sciences USA* 105, 4044-4049.

Bernhardt C, Lee MM, González A, Zhang F, Lloyd A, Schiefelbein J. 2003. The bHLH genes *GLABRA3* (*GL3*) and *ENHANCER OF GLABRA3* (*EGL3*) specify epidermal cell fate in the *Arabidopsis* root. *Development* 130, 6431-6439.

Bernhardt C, Zhao M, González A, Lloyd A, Schiefelbein J. 2005. The bHLH genes *GL3* and *EGL3* participate in an intercellular regulatory circuit that controls cell patterning in the *Arabidopsis* root epidermis. *Development* 132, 291-298.

Bourdenx B, Bernard A, Domergue F, Pascal S, Léger A, Roby D, *et al.* 2011. Overexpression of *Arabidopsis ECERIFERUM1* promotes was very-long-chain alcane biosynthesis and influences plant response to biotic and abiotic stress. *Plant Physiology* 156, 29-45.

Bray NL, Pimentel H, Melsted P, Pachter L. 2016. Near-optimal probabilistic RNA-seq quantification. *Nature Biotechnology* 34, 525-528.

Byrne ME, Barley R, Curtis M, Arroyo JM, Dunham M, Hudson A, Martienssen RA. 2000. Asymmetric leaves1 mediates leaf patterning and stem cell function in *Arabidopsis. Nature* 408, 967-971.

Chalvin C, Drevensek S, Dron M, Bendahmane A, Boualem A. 2020. Genetic control of glandular trichome development. *Trends in Plant Science* 25, 477-487.

Chen Z, Tan JLH, Ingouff M, Sundaresan V, Berger F. 2008. Chromatin assembly factor 1 regulates the cell cycle but not cell fate during male gametogenesis in *Arabidopsis thaliana*. *Development* 135, 65-73.

Davidson EH, Peter IS. 2015. Gene regulatory networks. In: Genomic control process. Elsevier. doi: 10.1016/B978-0-12-404729-7.00002

De Jager SM, Scofield S, Huntley RP, Robinson AS, den Boer BGW, Murray JAH. 2009. Dissecting regulatory pathways of G1/S control in *Arabidopsis*: common and distinct targets of CYCD3;1, E2Fa and E2Fc. *Plant Molecular Biology* 71, 345-365.

Di Stilio VS, Martin C, Schulfer AF, Connelly CF. 2009. An ortholog of *MIXTA*-like2 controls epidermal cell shape in flowers of *Thalictrum*. *The New Phytologist* 183, 718-728.

Digiuni S, Schellmann S, Geier F, Greese B, Pesch M, Wester K, *et al.* 2008. A competitive complex formation mechanism underlies trichome patterning on *Arabidopsis* leaves. *Molecular Systems Biology* 217, 1-11.

Dong Br, Wang Xx, Jiang R, Fang Sy, Li Jx, Li Q, Lv Zy, Chen Ws. 2021. *AaCycTL* regulates cuticle and trichome development in *Arabidopsis* and *Artemisia annua* L. *Frontiers in Plant Science* 12, 808283.

El Ottra JHL, Pirani JR, Endress JK. 2013. Fusion within and between whorls of floral organs in *Galipeinae* (Rutaceae): structural features and evolutionary implications. *Annals of Botany* 111, 821-837.

Erbar C, Heiler A, Leins P. 2016. Nectaries in fly-deceptive pitcher-trap blossoms of *Aristolochia*. *Flora* 232, 128-141.

Folkers U, Berger J, Hülskamp M. 1997. Cell morphogenesis of trichomes in *Arabidopsis*: differential control of primary and secondary branching by branch initiation regulators and cell growth. *Development* 124, 3779-3786.

Folkers U, Kirik V, Schöbinger U, Falk S, Krishnakumar S, Pollock MA, *et al.* 2002. The cell morphogenesis gene *ANGUSTIFOLIA* encodes a CtBP/BARS-like protein and is involved in the control of the microtubule cytoskeleton. *EMBO Journal* 15, 1280-1288.

Gan Y, Kumimoto R, Liu C, Ratcliffe O, Yu H, Broun P. 2006. GLABROUS INFLORESCENCE STEMS modulates the regulation by gibberellins of epidermal differentiation and shoot maturation in *Arabidopsis*. *The Plant Cell* 18, 1383-1395.

Gan Y, Liu C, Yu IL, Broun P. 2007. Integration of cytokinin and gibberellin signaling by *Arabidopsis* transcription factor GIS, ZFP8 and GIS2 in the regulation of epidermal cell fate. *Development* 134, 2073-2081.

Glover B J, Bunnewell S, Martin C. 2004. Convergent evolution within the genus *Solanum*: the specialized anther cone develops through alternative pathways. *Gene* 331, 1-7.

Han G, Li Y, Yang Z, Wang C, Zhang Y, Wang B. 2022. Molecular mechanisms of plant trichome development. *Frontiers in Plant Science* 13, 910228.

Hülskamp M, Miséra S, Jürgens G. 1994. Genetic dissection of trichome cell development in *Arabidopsis Cell* 76, 555-566.

Hülskamp M. 2004. Plant trichomes: a model for cell differentiation. *Nature Reviews Molecular Cell Biology* 5, 471-480.

Jaffé FW, Tattersall A, Glover BJ. 2007. A truncated MYB transcription factor from *Antirrhinum majus* regulates epidermal cell outgrowth. *Journal of Experimental Botany* 58, 1515-1524.

Jakoby MJ, Falkenhan D, Mader MT, Brininstool G, Wischnitzki E, Platz N, *et al.* 2008. Transcriptional profiling of mature *Arabidopsis* trichomes reveals that *NOECK* encodes the MIXTA-like transcriptional regulator MYB106. *Plant Physiology* 148, 1583-1602.

Imai KK, Ohashi Y, Tsuge T, Yoshizumi T, Matsui M, Oka A, *et al.* 2006. The A-type cyclin CYCA2;3 is a key regulator of ploidy levels in *Arabidopsis* endoreduplication. *The Plant Cell* 18, 382-396.

Ioannidi E, Rigas S, Tsitsekian D, Daras G, Alatzas A, Makris A, *et al.* 2016. Trichome patterning control involves TTG1 interaction with SPL transcription factors. *Plant Molecular Biology* 92, 675-687.

Kamata N, Okada H, Komeda Y, Takahashi T. 2013. Mutations in epidermis-specific HD-ZIP IV genes affect floral organ identity in *Arabidopsis thaliana*. *The Plant Journal* 75, 430-440.

Kang YH, Kirik V, Hülskamp M, Nam KH, Hagely K, Lee MM, *et al.* 2009. The *MYB23* gene provides a positive feedback loop for cell fate specification in the *Arabidopsis* root epidermis. *The Plant Cell* 21, 1080-1094.

Karabourniotis G, Papadopoulos K, Papamarkou M, Manetas Y. 1992. Ultraviolet-B radiation absorbing capacity of leaf hairs. *Physiologia Plantarum* 86, 414-418.

Kaya H, Shibahara KI, Taoka KI, Iwabuchi M, Stillman B, Araki T. 2001. *FASCIATA* genes for chromatin assembly factor-1 in *Arabidopsis* maintain the cellular organization of apical meristems. *Cell* 104, 131-142.

Khomtchouk BB, Hennessy JR, Wahlestedt C. 2017. Shinyheatmap: ultra-fast low memory heatmap web interface for big data genomics. *PLoS ONE* 12, e0176334.

Kirik V, Lee MM, Wester K, Herrmann U, Zheng Z, Oppenheimer D, *et al.* 2005. Functional diversification of *MYB23* and *GL1* genes in trichome morphogenesis and initiation. *Development* 132, 1477-1485.

Kirik V, Simon M, Hülskamp M, Schiefelbein J. 2004a. The *ENHANCER* of *TRY* and *CPC1* (*ETC1*) gene acts redundantly with TRIPTYCHON and CAPRICE in trichome and root hair cell patterning in *Arabidopsis*. *Developmental Biology* 268, 506-513.

Kirik V, Simon M, Wester K, Schiefelbein J, Hülskamp M. 2004b. ENHANCER of TRY and CPC2 (ETC2) reveals redundancy in the region-specific control of trichome development of *Arabidopsis. Plant Molecular Biology* 55, 389-398.

Kirik V, Lee MM, Wester K, Herrmann U, Zheng Z, Oppenheimer D, *et al.* 2005. Functional diversification of *MYB23* and *GL1* genes in trichome morphogenesis and initiation. *Development* 132, 1477-1485.

Koornneef M, Dellaert LWM, van der Veen JH. 1982. EMS- and radiation-induced mutation frequencies at individual loci in *Arabidopsis thaliana* (L) Heynh. *Mutation Research* 93, 109-123.

Krolikowski KA, Victor JL, Wagler TN, Lolle SJ, Pruitt RE. 2003. Isolation and characterization of the *Arabidopsis* organ fusion gene *HOTHEAD*. *The Plant Journal* 35, 501-511.

Kubo H, Peeters AJM, Aarts MGM, Pereira A, Koornneef M. 1999. *ANTHOCYANINLESS2*, a homeobox gene affecting anthocyanin distribution and root development in *Arabidopsis*. *The Plant Cell* 11: 1217-1226.

Kurdyukov S, Faust A, Trenkamp S, Bär S, Franke R, Efremova N, *et al.* (2006). Genetic and biochemical evidence for involvement of HOTHEAT in the biosynthesis of lon-chain alpha-, omega-dicarboxyl fatty acids and formation of extracellular matrix. *Planta* 224, 315-329.

Levin DA. 1973. The role of trichomes in plant defense. *Quarterly Review of Biology* 48, 3-15.

Li Q, Zhang C, Li J, Wang L, Ren Z. 2012. Genome-wide identification and characterization of R2R3MYB family in *Cucumis sativus*. *PloS One* 7, e47576.

Li YJ, Zhu SH, Zhang XY, Liu YC, Xue F, Zhao LJ, et al. 2017. Expression and functional analyses of a Kinesin gene *GhKIS13A1* from cotton (*Gossypium hirsutum*) fiber. *BMC Biotechnol*ogy 17, 50.

Liu X, Bartholomew E, Cai Y, Ren H. 2016. Trichome-related mutants provide a new perspective on multicellular trichome initiation and development in cucumber (*Cucumis sativus* L). *Frontiers in Plant Science* 7, 1187.

Liu S, Jiao J, Lu TJ, Xu F, Pickard BG, Genin GM. 2017. *Arabidopsis* leaf trichomes as acoustic antennae. *Biophysical Journal* 113, 2068-2076.

Livak KJ, Schmittgen TD. 2001. Analysis of relative gene expression data using real-time quantitative PCR and the $2^{-\Delta\Delta Ct}$ method. *Methods* 52, 402-408.

Lu L, Lee YRJ, Pan R, Maloof JN, Liu B. 2005. An internal motor kinesin is associated with the Golgi apparatus and plays a role in trichome morphogenesis in *Arabidopsis*. *Molecular Biology of the Cell* 16, 811-823.

Lü S, Song T, Kosma DK, Parsons EP, Rowland O, Jenks MA. 2009. *Arabidopsis* CER8 encodes LONG-CHAIN ACYL-COA SYNTHETASE1 (LACS1) that has overlapping functions with LACS2 in plant wax and cutin synthesis. *The Plant Cell* 59, 553-564.

Mabuchi A, Soga K, Wakabayashi K, Hoson T. 2016. Phenotypic screening of *Arabidopsis* T-DNA insertion lines for cell wall mechanical properties revealed *ANTHOCYANINLESS2*, a cell wall-related gene. *Journal of Plant Physiology* 191, 29-35.

Machida C, Nakagawa A, Kojima S, Takahashi H, Machida Y. 2015. The complex of ASYMMETRIC LEAVES (AS) proteins plays a central role in antagonistic interactions of genes for leaf polarity specification in *Arabidopsis. Wiley Interdisciplinary Reviews. Developmental Biology* 4, 655-671.

Marks MD, Esch JJ. 1994. Morphology and development of mutant and wild type trichomes on the leaves of *Arabidopsis thaliana*. In *Arabidopsis*: An atlas of morphology and development. (Ed. J. Bowman), pp. 56-73. New York: Springer-Verlag.

Matías-Hernández L, Aguilar-Jaramillo AE, Osnato M, Weinstain R, Shani E, Suárez-López P, Pelaz S. 2016. TEMPRANILLO reveals the mesophyll as crucial for epidermal trichome formation. *Plant Physiology* 170, 1624-1639.

Mathur J, Chua NH. 2000. Microtubule stabilization leads to growth reorientation in *Arabidopsis* trichomes. *The Plant Cell* 12, 465-477.

Mathur, J., Spielhofer, P., Kost, B., and Chua, N. H. (1999). The actin cytoskeleton is required to elaborate and maintain spatial patterning during trichome cell morphogenesis in *Arabidopsis thaliana. Development* 126, 5559-5568.

Nadakuduti SS, Pollard M, Kosma DK, Allen JrC, Ohlrogge JB, Barry CS. 2012. Pleiotropic phenotypes of the sticky peel mutant provide new insight into the role of CUTIN DEFICIENT2 in epidermal cell function in tomato. *Plant Physiology* 159, 945-960.

Noda K, Glover BJ, Linstead P, Martin C. 1994. Flower colour intensity depends on specialized cell shape controlled by a Myb-related transcription factor. *Nature* 369, 661-664.

Oelschlägel B, Gorb S, Wanke S, Neinhuis C. 2009. Structure and biomechanics of trapping flower trichomes and their role in the pollination biology of *Aristolochia* plants (Aristolochiaceae). *New Phytologist* 184, 988-1002.

Oppenheimer DG, Herman PL, Sivakumaran S, Esch J, Marks MD. 1991. A *myb* gene required for leaf trichome differentiation in *Arabidopsis* is expressed in stipules. *Cell* 67, 483-493.

Oppenheimer DG, Pollock MA, Vacik J, Szymanski DB, Ericson B, Feldmann K, *et al.* 1997. Essential role of a kinesin-like protein in *Arabidopsis* trichome morphogenesis. *Proceedings of the National Academy of Sciences USA* 94, 6261-6266.

Pabón-Mora N, Suárez-Baron H, Ambrose BA, González F. 2015. Flower development and perianth identity candidate genes in the basal angiosperm *Aristolochia fimbriata* (Piperales: Aristolochiaceae). *Frontiers in Plant Science* 6, 1095.

Pascal S, Bernard A, Deslous P, Gronnier J, Fournier-Goss A, Domergue F, *et al.* 2019. *Arabidopsis* CER1-LIKE1 functions in a cuticular very-long-chain alkane-forming complex. *Plant Physiology* 179, 415-432.

Pattanaik S, Patra B, Singh SK, Yuan L. 2014. An overview of the gene regulatory network controlling trichome development in the model plant, *Arabidopsis. Frontiers in Plant Science* 5, 259.

Payne T, Clement J, Arnold D, Lloyd A. 1999. Heterologous myb genes distinct from GL1 enhance trichome production when overexpressed in *Nicotiana tabacum. Development* 126, 671-682.

Payne CT, Zhang F, Lloyd AM. 2000. *GL3* encodes a bHLH protein that regulates trichome development in Arabidopsis through interaction with GL1 and TTG1. *Genetics* 156, 1349-1362.

Perazza, D., Vachon, G., and Herzog, M. (1998. Gibberellins promote trichome formation by up-regulating GLABROUS1 in *Arabidopsis*. *Plant Physiology* 117, 375-383.

Pérez-Rodríguez M, Jaffé FW, Butelli E, Glover BJ, Martin C. 2005. Development of three different cell types is associated with the activity of a specific MYB transcription factor in the ventral petal of *Antirrhinum majus* flowers. *Development* 132, 359-370.

Perrin RM, Wang Y, Yuen CYL, Will J, Masson PH. 2007. WVD2 is a novel microtubule-associated protein in *Arabidopsis thaliana. The Plant Journal* 49, 961-971.

Qi T, Song S, Ren Q, Wu D, Huang H, Chen Y, *et al.* 2011. The jasmonate ZIM-domain proteins interact with the WD-repeat/bHLH/MYB complexes to regulate jasmonate-mediated anthocyanin accumulation and trichome initiation in *Arabidopsis thaliana. The Plant Cell* 23, 1795-1814.

Qin W, Xie L, Li Y, Liu H, Fu X, Chen T, Hassani D, Li L, Sun X, Tang K. 2021. An R2R3-MYB transcription factor positively regulates the glandular secretory trichome initiation in *Artemisia annua. Frontiers in Plant Science* 12, 657156.

Qiu JL, Jilk R, Marks MD, Szymanski DB. 2002. The *Arabidopsis SPIKE1* gene is required for normal cell shape control and tissue development. *The Plant Cell* 14, 101-118.

Rerie WG, Feldmann KA, Marks MD. 1994. The *GLABRA2* gene encodes a homeodomain protein required for normal trichome development in *Arabidopsis*. *Genes & Development* 8, 1388-1399.

Sambade A, Findlay K, Schäffner AR, Lloyd CW, Buschmann H. 2014. Actin-dependent and -independent functions of cortical microtubules in the differentiation of *Arabidopsis* leaf trichomes. *The Plant Cell* 26, 1629-1644.

Schnittger A, Hülskamp M. 2002. Trichome morphogenesis: a cell-cycle perspective. *Philosophical Transactions of the Royal Society B: Biological Sciences* 357, 823-826.

Schellmann S, Hülskamp M. 2005. Epidermal differentiation: trichomes in *Arabidopsis* as a model system. *The International Journal of Developmental Biology* 49, 579-584.

Schellmann S, Schnittger A, Kirik V, Wada T, Okada K, Beermann A, *et al.* 2002. TRIPTYCHON and CAPRICE mediate lateral inhibition during trichome and root hair patterning in *Arabidopsis. EMBO Journal* 21, 5036-5046.

Schnittger A, Folkers U, Schwab B, Jürgens G, Hülskamp M. 1999. Generation of a spacing pattern: the role of TRIPTYCHON in trichome patterning in *Arabidopsis. The Plant Cell* 11, 1105-1116.

Schnittger A, Hülskamp M. 2002. Trichome morphogenesis: a cell-cycle perspective. *Philosophical Transactions of the Royal Society B: Biological Sciences* 357, 823-826.

Smith LG, Oppenheimer DG. 2005. Spatial control of cell expansion by the plant cytoskeleton. *Annual Review of Cell and Developmental Biology* 21, 271-295.

Sozzani R, Maggio C, Varotto S, Canova S, Bergounioux C, Albani D, *et al.* 2006. Interplay between *Arabidopsis* activating factors E2Fb and E2Fa in cell cycle progression and development. *Plant Physiology* 140, 1355-1366.

Stracke R, Werber M, Weisshaar B. 2001. The R2R3-MYB gene family in *Arabidopsis thaliana. Current Opinion in Plant Biology* 4, 447-456.

Suárez-Baron H, Alzate JF, González F, Ambrose BA, Pabón-Mora N. 2019. Genetic mechanisms underlying perianth epidermal elaboration of *Aristolochia ringens* Vahl (Aristolochiaceae). *Flora* 253: 56-66.

Suárez-Baron H, Alzate JF, González F, Pelaz S, Ambrose BA, Pabón-Mora N. 2021. Gene expression underlying floral epidermal specialization in *Aristolochia fimbriata* (Aristolochiaceae). *Annals of Botany* 127, 749-764.

Sun Y, Zhou Q, Zhang W, Fu Y, Huang H. 2002. *ASYMMETRIC LEAVES1*, an *Arabidopsis* gene that is involved in the control of cell differentiation in leaves. *Planta* 214, 694-702.

Szklarczyk D, Morris JH, Cook H, Kuhn M, Wyder S, Simonovic M, *et al.* 2017. The STRING database in 2017: quality-controlled protein-protein association networks, made broadly accessible. *Nucleic Acids Research* 45, D362-D368.

Szymanski DB. 2009. Plant cells taking shape: new insight into cytoplasmic control. *Current Opinion in Plant Biology* 12, 735-744.

Tan J, Walford SA, Dennis ES, Llewellyn D. 2016. Trichomes control flower bud shape by linking together young petals. *Nature Plants* 2, 16093.

Tian J, Han L, Feng Z, Wang G, Liu W, Ma Y, *et al.* 2015. Orchestration of microtubules and the actin cytoskeleton in trichome cell shape determination by a plant-unique kinesis. *eLife* 4, 09351.

Tominaga R, Iwata M, Sano R, Inoue K, Okada K, Wada T. 2008. *Arabidopsis CAPRICE-LIKE MYB 3* (*CPL3*) controls endoreduplication and flowering development in addition to trichome and root hair formation. *Development* 135, 1335-1345.

Traw MB, Bergelson J. 2003. Interactive effects of jasmonic acid, salicylic acid, and gibberellin on induction of trichomes in *Arabidopsis. Plant Physiology* 133, 1367-1375.

Wagner GJ. 1991. Secreting glandular trichomes: more than just hairs. *Plant Physiology* 96, 675-679.

Wagner GJ, Wang E, Shepherd RW. 2004. New approaches for studying and exploiting and old protuberance, the plant trichome. *Annals of Botany* 93, 3-11.

Walker AR, Davison PA, Bolognesi-Winfield AC, James CM, Srinivasan N, Blundell TL, *et al.* 1999. The *TRANSPARENT TESTA GLABRA1* locus, which regulates trichome differentiation and anthocyanin biosynthesis in *Arabidopsis,* encondes a WD40 repeat protein. *The Plant Cell* 11, 1337-1349.

Wang X, Shen C, Meng P, Tan G, Litang Lv. 2021. Analysis and review of trichomes in plants. *BMC Plant Biology* 70: 1-11.

Wang S, Kwak SH, Zeng Q, Ellis BE, Chen XY, Schiefelbein J, *et al.* 2007. *TRICHOMELESS1* regulates trichome patterning by suppressing *GLABRA1* in *Arabidopsis*. *Development* 134, 3873-3882.

Yanagisawa M, Alonso JM, Szymasnki DB. 2018. Microtubule-depending confinement of a cell signaling and actin polymerization control module regulates polarized cell growth. *Current Biol*ogy 28, 1-8.

Yanagisawa M, Desyatova AS, Belteton SA, Mallery EL, Turner JA, Szymanski DB. 2015. Patterning mechanisms of cytoskeletal and cell wall systems during leaf trichome morphogenesis. *Nature Plants* 1, 1-8.

Yang C, Li H, Zhang J, Luo Z, Gong P, Zhang C, *et al.* 2011. Fine-mapping of the woolly gene controlling multicellular trichome formation and embryonic development in tomato. *Theoretical and Applied Genetics* 123, 625-633.

Yang S, Cai Y, Liu X, Dong M, Zhang Y, Chen S, *et al.* 2018. A *CsMYB6-CsTRY* module regulates fruit trichome initiation in cucumber. *Journal of Experimental Botany* 69, 1887-1902.

Yang C, Ye Z. 2013. Trichomes as models for studying plant cell differentiation. *Cellular and Molecular Life Sciences* 70, 1937-1948.

Yang C, Gao Y, Gao S, Yu G, Xiong C, Chang J, *et al*. 2015. Transcriptome profile analysis of cell proliferation molecular processes during multicellular trichome formation induced by tomato *Wo*^{v} gene in tobacco. *Genomics* 16, 868.

Yoshida Y, Sano R, Wada T, Takabayashi J, Okada, K. 2009. Jasmonic acid control of GLABRA3 links inducible defense and trichome patterning in *Arabidopsis. Development* 136, 1039-1048.

Yuen CYL, Pearlman, RS, Silo-suh L, Hilson P, Carroll KL, Masson PH. 2003. WVD2 and WDL1 modulate helical organ growth and anisotropic cell expansion in *Arabidopsis. Plant Physiology* 131, 493-506.

Zhang C, Kotchoni SO, Samuels AL, Szymanski D. B. 2010. SPIKE1 signals originate from and assemble specialized domains of the endoplasmic reticulum. *Current Biology* 20, 2144-2149.

Zhang F, Gonzalez A, Zhao M, Payne CT, Lloyd A. 2003. A network of redundant bHLH proteins functions in all TTG1-dependent pathways of *Arabidopsis. Development* 130, 4859-4869.

Zhao M, Morohashi K, Hatlestad G, Grotewold E, Lloyd A. 2008. The TTG1-bHLH-MYB complex controls trichome cell fate and patterning through direct targeting of regulatory loci. *Development* 135, 1991-1999.

Zhao JL, Pan JS, Guan Y, Nie JT, Yang JJ, Qu ML, *et al*. 2015a. Transcriptome analysis in *Cucumis sativus* identifies genes involved in multicellular trichome development. *Genomics* 105, 296-303.

Zhao JL, Pan JS, Guan Y, Zhang WW, Bie BB, Wang YL, *et al*. 2015b. Micro-trichome as a class I homeodomain-leucine zipper gene regulates multicellular trichome development in *Cucumis sativus. Journal of Integrative Plant Biology* 57, 925-935.

Zhou Z, Sun L, Zhao Y, An L, Yan A, Meng X, Gan Y. 2013. *Zinc Finger Protein 6* (*ZFP6*) regulates trichome initiation by integrating gibberellin and cytokinin signaling in *Arabidopsis thaliana. New Phytologist* 198, 699-708.

Zhou LH, Liu SB, Wang PF, Lu TJ, Xu F, Genin GM, *et al*. 2016. The *Arabidopsis* trichome is an active mechanosensory switch. *Plant Cell and Environment* 40, 611-621.

Zhu Y, Weng M, Yang Y, Zhang C, Li Z, Shen WH, *et al*. 2011. *Arabidopsis* homologues of the histone chaperone ASF1 are crucial for chromatin replication and cell proliferation in plant development. *The Plant Journal* 66, 443-455.

Zimmermann IM, Heim MA, Weisschaar B, Uhrig JE. 2004. Comprehensive identification of *Arabidopsis thaliana* MYB transcription factors integrating with R/B-like bHLH proteins. *The Plant Journal* 40, 22-34.

Figure legends

Figure 1. Schematic representation of trichomes development in the perianth of *Aristolochia fimbriata*. Development of the three-celled hooked (uncinate) trichomes in the limb **(A)**, secretory conical trichomes in the tube **(B)**, and filamentous multicellular trichomes in the utricle **(C)**. Trichome differentiation was characterized by six stages of development. Stage 1 stands for the initiation of a trichome precursor cell while stage 6 indicates a mature trichome. Trichome stage 3 corresponds to the S6 floral stage and stage 6 to the S9 (preanthetic flower). **Scale Bars: (A)**: 20 μm; **(B-C)**: 40 μm.

Figure 2. Morphoanatomical characterization of the *Aristolochia fimbriata* perianth. (A) Floral buds at stage S6 showing outer (left) and inner (mid) surfaces and the gynostemium (right) **(B)** Floral buds at S9 showing outer (left) and inner (mid) surfaces and the gynostemium (right) **(C)** Flower at anthesis. (**D-G)** Transverse sections of the limb at S6 **(D, E)** and S9 **(F, G)**; note hooked trichome development in the inner epidermis. **(H-K)** Transverse sections of the tube at S6 **(H, I)** and S9 **(J, K)**; note the secretory conical trichome development in the inner epidermis. **(L-O)** Transverse sections of the utricle at S6 **(L, M)** and S9 **(N, O)**; note the filamentous multicellular trichome development. Arrowheads point to trichomes in the perianth, arrows point to stigmatic lobes, asterisks indicate anthers; fi, fimbriae; g, gynostemium; ie, inner epidermis; oe, outer epidermis; o, ovary; l, limb; t, tube; u, utricle. **Scale Bars: (A)**: 0.5 cm; **(B, C)**: 1 cm; **(D, F, H, J, L, N)**: 100 μm; **(E, G, I, K, M, O)**: 50 μm.

Figure 3. Morphoanatomical characterization of the *Aristolochia macrophylla* perianth. (A) Floral buds at S6 showing outer (left) and inner (mid) surfaces and the gynostemium (right) **(B)** Floral buds at S9 showing outer (left) and inner (mid) surfaces and the gynostemium (right) **(C)** Flower at anthesis. (**D-G)** Transverse sections of the limb at S6 **(D, E)** and S9 **(F, G)**; note the absence of trichomes in the inner epidermis. **(H-K)** Transverse sections of the tube at S6 **(H, I)** and S9 **(J, K)**; note the absence of trichomes in the inner epidermis. **(L-O)** Transverse sections of the utricle at S6 **(L, M)** and S9 **(N, O)**; note the filamentous multicellular trichomes developing. Arrowheads point to trichomes in the perianth, arrows point to stigmatic lobes and asterisks indicate anthers; fi, fimbriae; g, gynostemium; ie, inner epidermis; oe, outer epidermis; o, ovary; l, limb; t, tube; u, utricle. **Scale Bars: (A)**: 0.5 cm; **(B, C)**: 1 cm; **(D, F, H, J, L, N)**: 100 μm; **(E, G, I, K, M, O)**: 50 μm.

Figure 4. Epidermal differentiation of the three perianth regions in *Aristolochia fimbriata* (A-H) and *Aristolochia macrophylla* (I-P Q). **(A)** *A. fimbriata* preanthetic flower at S9, sagittal section. **(B-C)** inner **(B)** and outer **(C)** limb epidermis. **(D-E)** inner **(D)** and outer **(E)** tube epidermis. **(F-G)** inner **(F)** and outer **(G)** utricle epidermis. **(H)** Anthetic flower. **(I)** *A. macrophylla* preanthetic flower at S9, sagittal section. **(J-K)** inner **(J)** and outer **(K)** limb epidermis. **(L-M)** inner **(L)** and outer **(M)** tube epidermis. **(N-O)** inner **(N)** and outer **(O)**

utricle epidermis. **(P)** Anthetic flower. Arrowheads point to trichomes. f, fimbriae; g, gynostemium; ie, inner epidermis; oe, outer epidermis; o, ovary; l, limb; t, tube; u, utricle. **Scale Bars: (A, H, I, Q)**: 1 cm; **(B, D, F, K, M, O, P)**: 100 μm; **(C, E, G, J, L)**: 50 μm.

Figure 5. Trichome-related gene expression heat map in *Aristolochia fimbriata*. Hierarchical clustering heat map showing expression data of 82 trichome-related genes in the limb, tube and utricle of *Aristolochia fimbriata* at stages S6 and S9. Genes are displayed in rows with normalized transcripts per million (TPMs) values for the comparisons. Gene expression levels follow the row *z* score convention at the top left with red indicating upregulation and green indicating downregulation. The black arrow points to a cluster of genes highly expressed in the perianth at the early stage (S6).

Figure 6. Differential gene expression in *Aristolochia fimbriata* and *Aristolochia macrophylla*. Total number of Differentially Expressed Genes (DEGs) in pairwise comparisons at two different developmental stages (S6 and S9) in three different perianth regions: the limb, the tube, and the utricle in *A. fimbriata* **(A)** and *A. macrophylla* **(B)**. Values above columns represent total number of DEGs.

Figure 7. Hierarchical clustering heat maps of top 60 differentially expressed genes (DEGs) in the perianth of *Aristolochia fimbriata.* The genes are displayed in rows with normalized transcripts per million (TPMs) values for the comparisons Limb at S6 *versus* S9 developmental stage **(A)**. Tube at S6 *versus* S9 stage **(B)**. Utricle at S6 *versus* S9 **(C)**. Each sample has three biological replicates. Gene expression levels are denoted at the top of the heatmap, with red and green indicating up-regulated and down-regulated expression, respectively.

Figure 8. Hypothetical gene regulatory network (GRN) and hormone signaling underlying cell fate and trichome development in the *Aristolochia* perianth. The putative activators of trichome initiation include AfimMYB23, AfimWIN1, and AfimMYB106-like. Then AfimGL2 or AfimHDG2 are activated, which in turn activates other transcription factors, such as *AfimRAV*-like might be also regulating an additional activation pathway of trichome development through the regulation of that trimeric complex. Negative regulation of trichome fate consists of the combined activity of AfimMYB6 and AfimETC3 (R3-MYB); AfimETC might be moving to the neighboring cells (red dash arrow). Gibberellins (GAs) and Cytokinins (CKs) contribute positively to the regulation of trichome development. GAs can stimulate the transcription of the *ZINC FINGER PROTEIN 6* (*AfimZFP6*) gene, and then AfimZFP6 might be inducing the expression of *AfimZFP8*, and *AfimZFP8* may control *AfimGL2*/*AfimHDG2*. AfimSPK1 might be controlling *AfimRBR1* and then modulating different pathways of trichome maturation by controlling different genes related to cell cycle progression, cell polarity, and cytoskeleton dynamics (i. e.: *AfimCDKs, AfimKINs*, and *AfimARPs*).

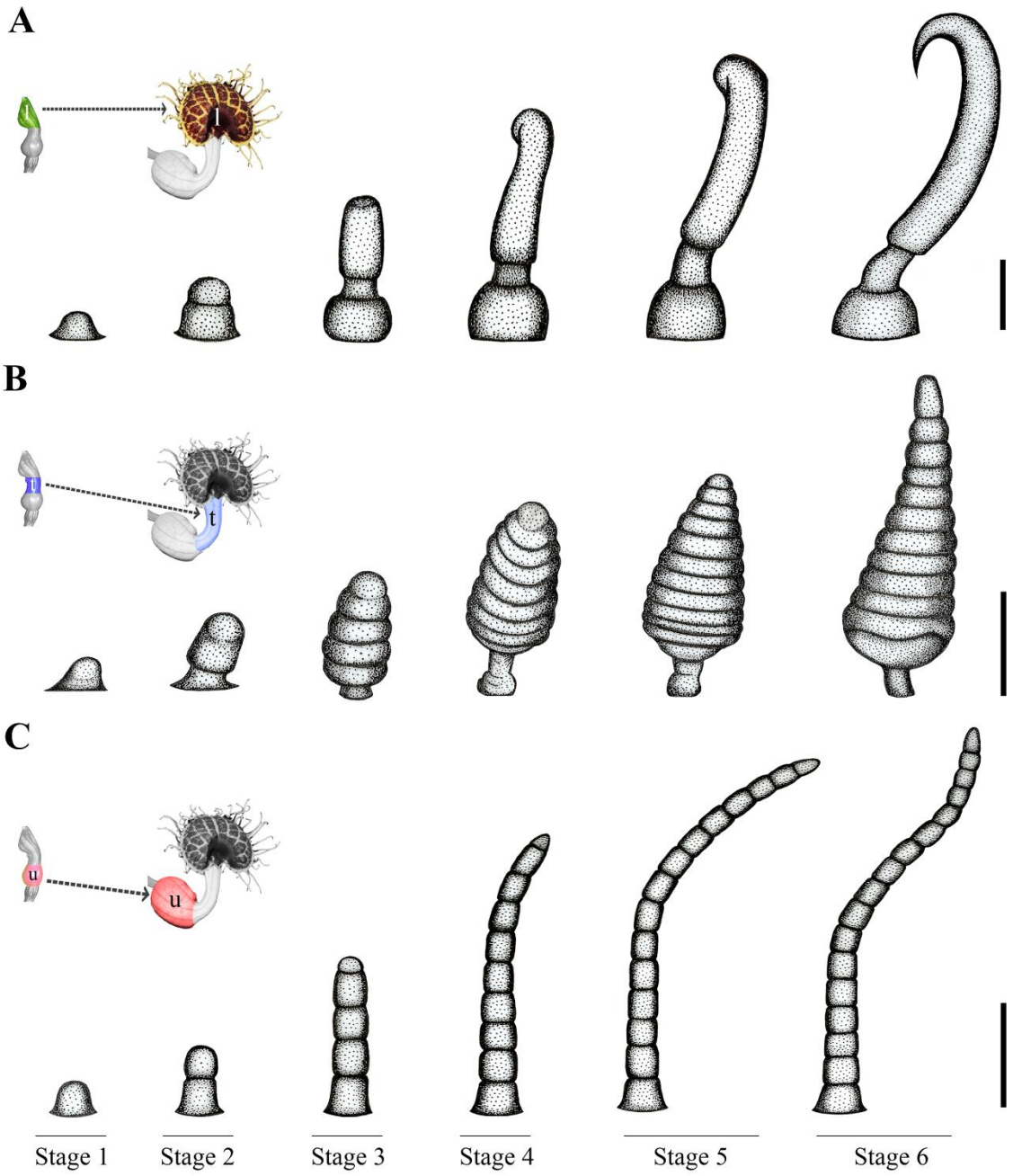

Figure 1. Schematic representation of trichomes development in the perianth of Aristolochia fimbriata. Development of the three-celled hooked (uncinate) trichomes in the limb (A), secretory conical trichomes in the tube (B), and filamentous multicellular trichomes in the utricle (C). Trichome differentiation was characterized by six stages of development. Stage 1 stands for the initiation of a trichome precursor cell while stage 6 indicates a mature trichome. Trichome stage 3 corresponds to the S6 floral stage and stage 6 to the S9 (preanthetic flower). Scale Bars: (A): 20 μm; (B-C): 40 μm.

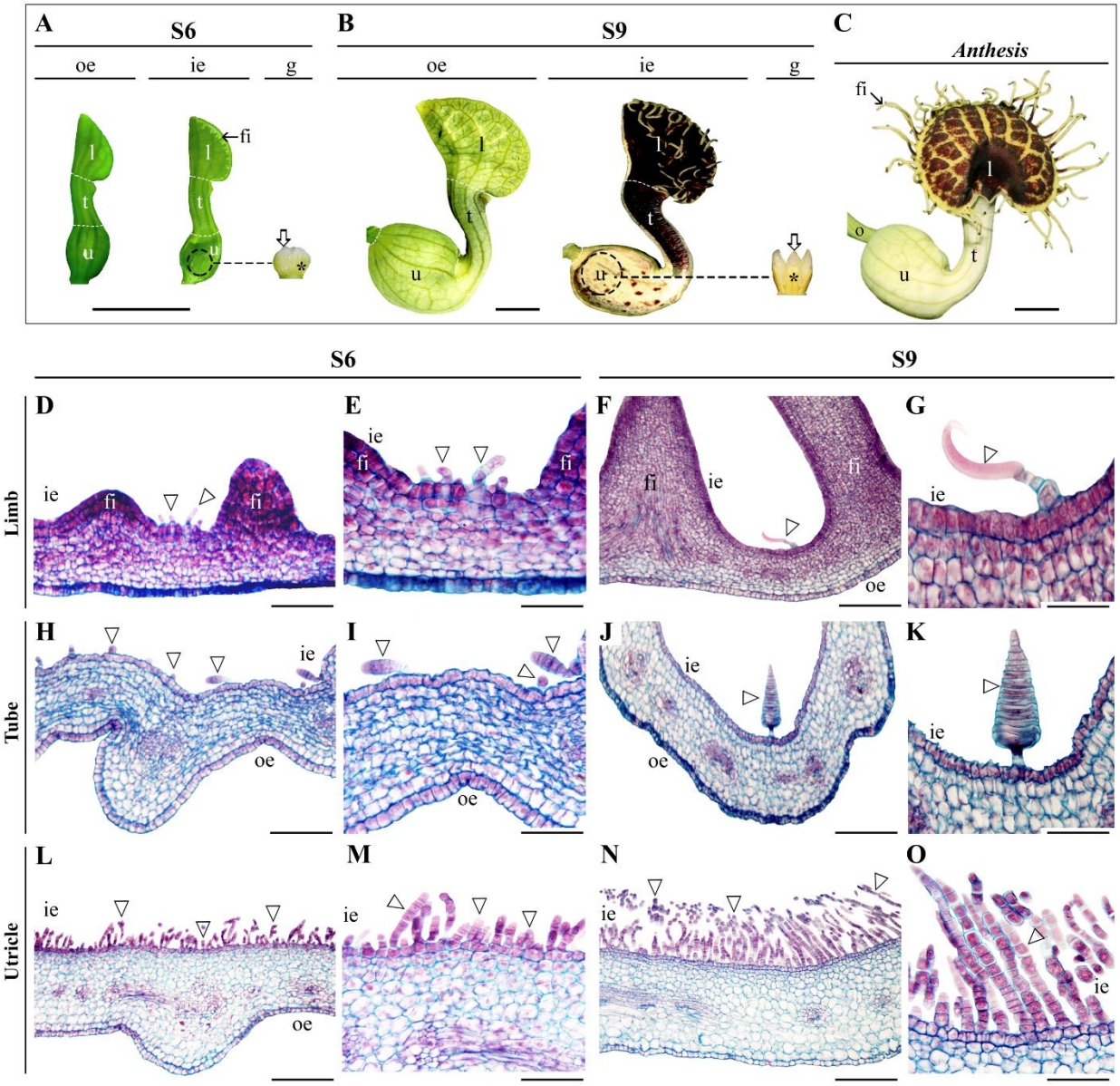

Figure 2. Morphoanatomical characterization of the Aristolochia fimbriata perianth. (A) Floral buds at stage S6 showing outer (left) and inner (mid) surfaces and the gynostemium (right) (B) Floral buds at S9 showing outer (left) and inner (mid) surfaces and the gynostemium (right) (C) Flower at anthesis. (D-G) Transverse sections of the limb at S6 (D, E) and S9 (F, G); note hooked trichome development in the inner epidermis. (H-K) Transverse sections of the tube at S6 (H, I) and S9 (J, K); note the secretory conical trichome development in the inner epidermis. (L-O) Transverse sections of the utricle at S6 (L, M) and S9 (N, O); note the filamentous multicellular trichome development. Arrowheads point to trichomes in the perianth, arrows point to stigmatic lobes, asterisks indicate anthers; fi, fimbriae; g, gynostemium; ie, inner epidermis; oe, outer epidermis; o, ovary; l, limb; t, tube; u, utricle. Scale Bars: (A): 0.5 cm; (B, C): 1 cm; (D, F, H, J, L, N): 100 μm; (E, G, I, K, M, O): 50 μm.

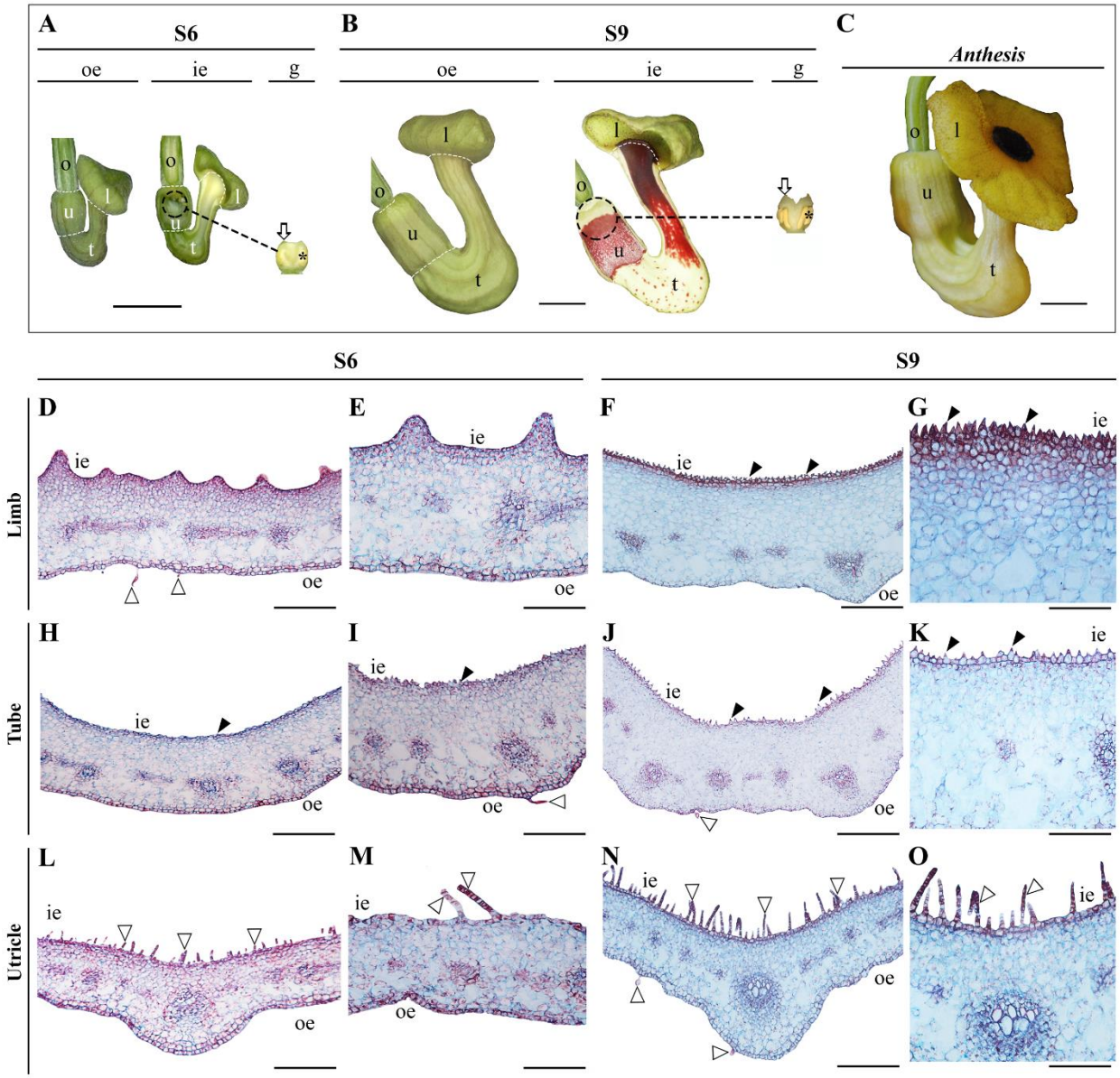

Figure 3. Morphoanatomical characterization of the Aristolochia macrophylla perianth. (A) Floral buds at S6 showing outer (left) and inner (mid) surfaces and the gynostemium (right) (B) Floral buds at S9 showing outer (left) and inner (mid) surfaces and the gynostemium (right) (C) Flower at anthesis. (D-G) Transverse sections of the limb at S6 (D, E) and S9 (F, G); note the absence of trichomes in the inner epidermis. (H-K) Transverse sections of the tube at S6 (H, I) and S9 (J, K); note the absence of trichomes in the inner epidermis. (L-O) Transverse sections of the utricle at S6 (L, M) and S9 (N, O); note the filamentous multicellular trichomes developing. Arrowheads point to trichomes in the perianth, arrows point to stigmatic lobes and asterisks indicate anthers; fi, fimbriae; g, gynostemium; ie, inner epidermis; oe, outer epidermis; o, ovary; l, limb; t, tube; u, utricle. Scale Bars: (A): 0.5 cm; (B, C): 1 cm; (D, F, H, J, L, N): 100 μm; (E, G, I, K, M, O): 50 μm.

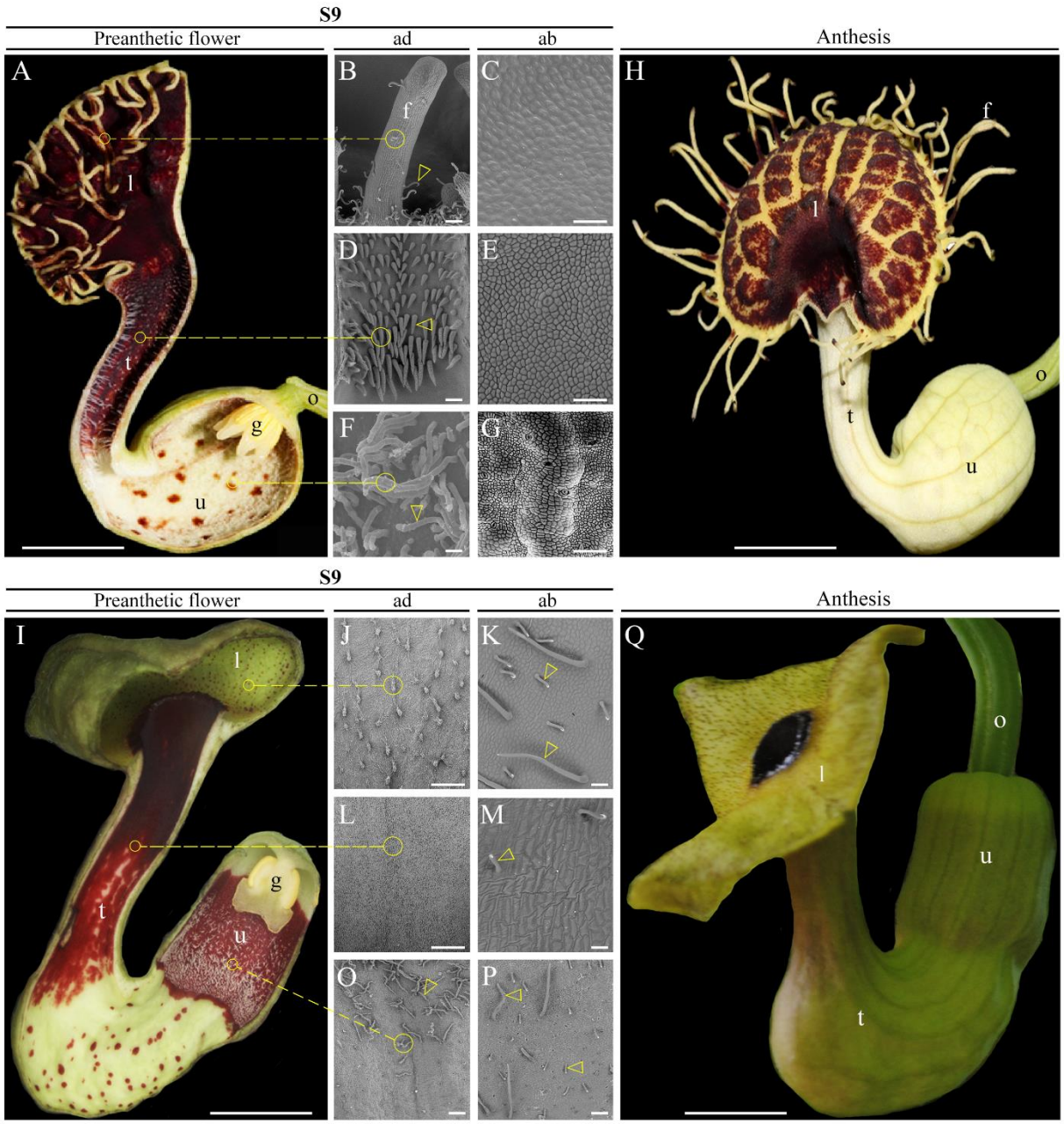

Figure 4. Epidermal differentiation of the three perianth regions in Aristolochia fimbriata (A-H) and Aristolochia macrophylla (I-P Q). (A) A. fimbriata preanthetic flower at S9, sagittal section. (B-C) inner (B) and outer (C) limb epidermis. (D-E) inner (D) and outer (E) tube epidermis. (F-G) inner (F) and outer (G) utricle epidermis. (H) Anthetic flower. (I) A. macrophylla preanthetic flower at S9, sagittal section. (J-K) inner (J) and outer (K) limb epidermis. (L-M) inner (L) and outer (M) tube epidermis. (N-O) inner (N) and outer (O) utricle epidermis. (P) Anthetic flower. Arrowheads point to trichomes. f, fimbriae; g, gynostemium; ie, inner epidermis; oe, outer epidermis; o, ovary; l, limb; t, tube; u, utricle. Scale Bars: (A, H, I, Q): 1 cm; (B, D, F, K, M, O, P): 100 μm; (C, E, G, J, L): 50 μm.

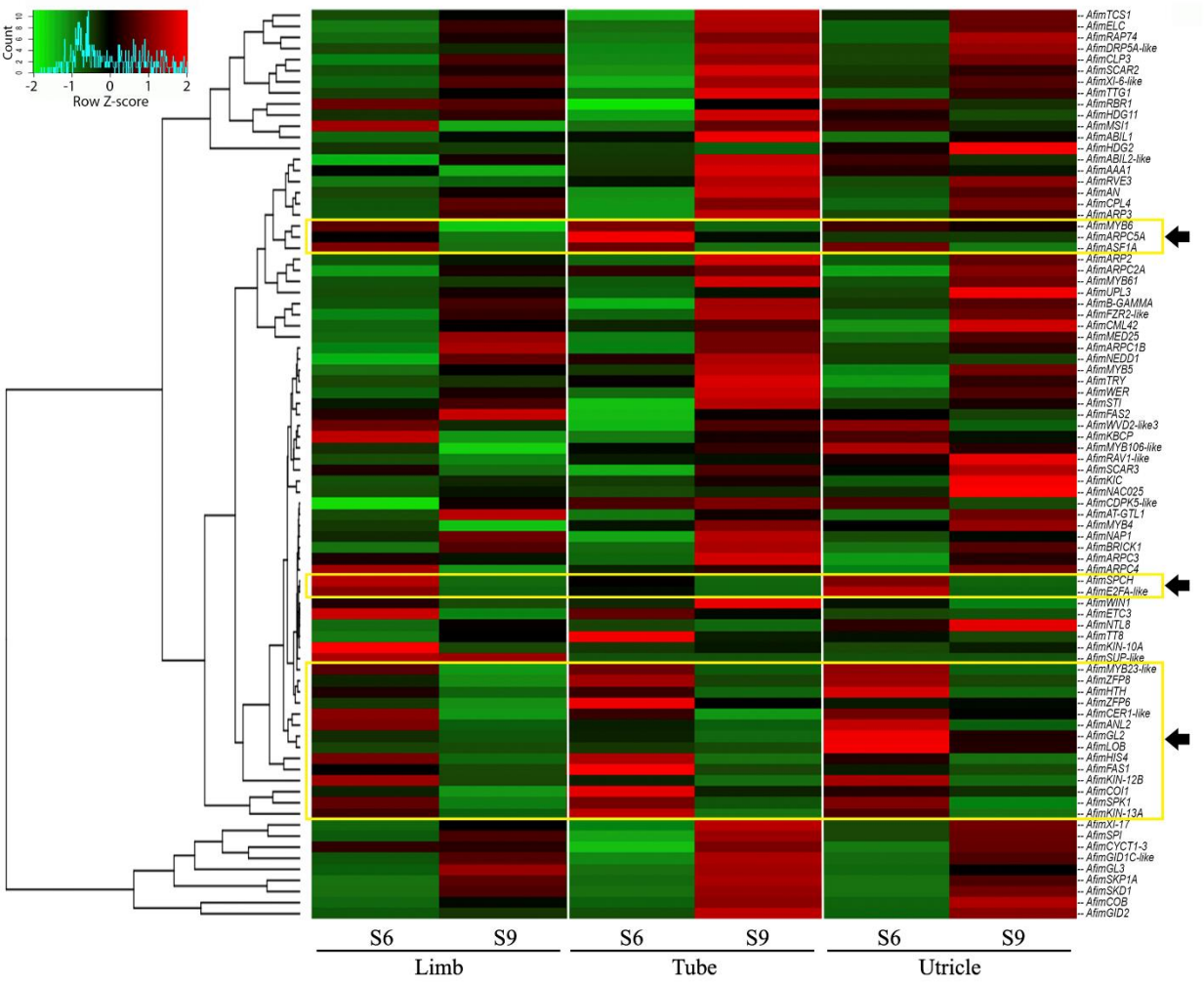

Figure 5. Trichome-related gene expression heat map in Aristolochia fimbriata. Hierarchical clustering heat map showing expression data of 82 trichome-related genes in the limb, tube and utricle of Aristolochia fimbriata at stages S6 and S9. Genes are displayed in rows with normalized transcripts per million (TPMs) values for the comparisons. Gene expression levels follow the row z score convention at the top left with red indicating upregulation and green indicating downregulation. The black arrow points to a cluster of genes highly expressed in the perianth at the early stage (S6).

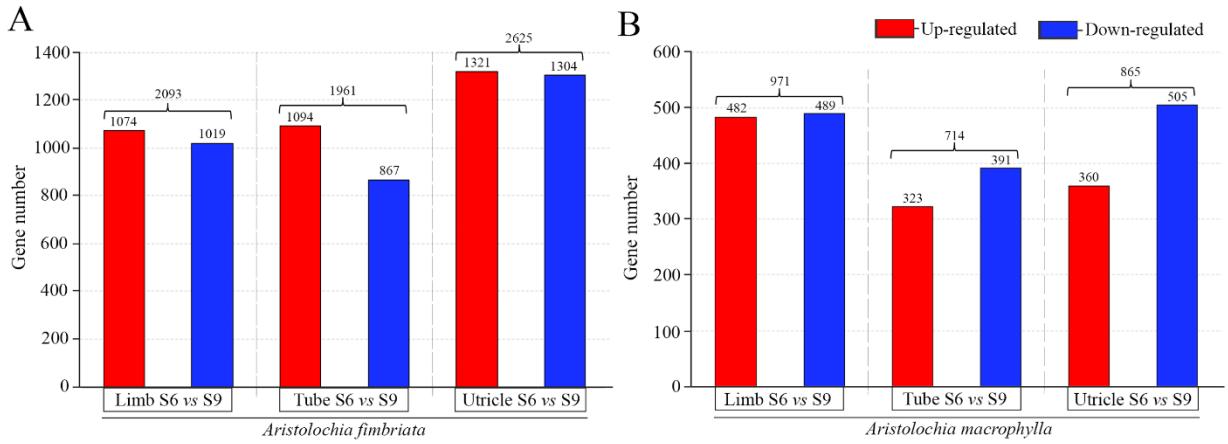

Figure 6. Differential gene expression in Aristolochia fimbriata and Aristolochia macrophylla. Total number of Differentially Expressed Genes (DEGs) in pairwise comparisons at two different developmental stages (S6 and S9) in three different perianth regions: the limb, the tube, and the utricle in A. fimbriata (A) and A. macrophylla (B). Values above columns represent total number of DEGs.

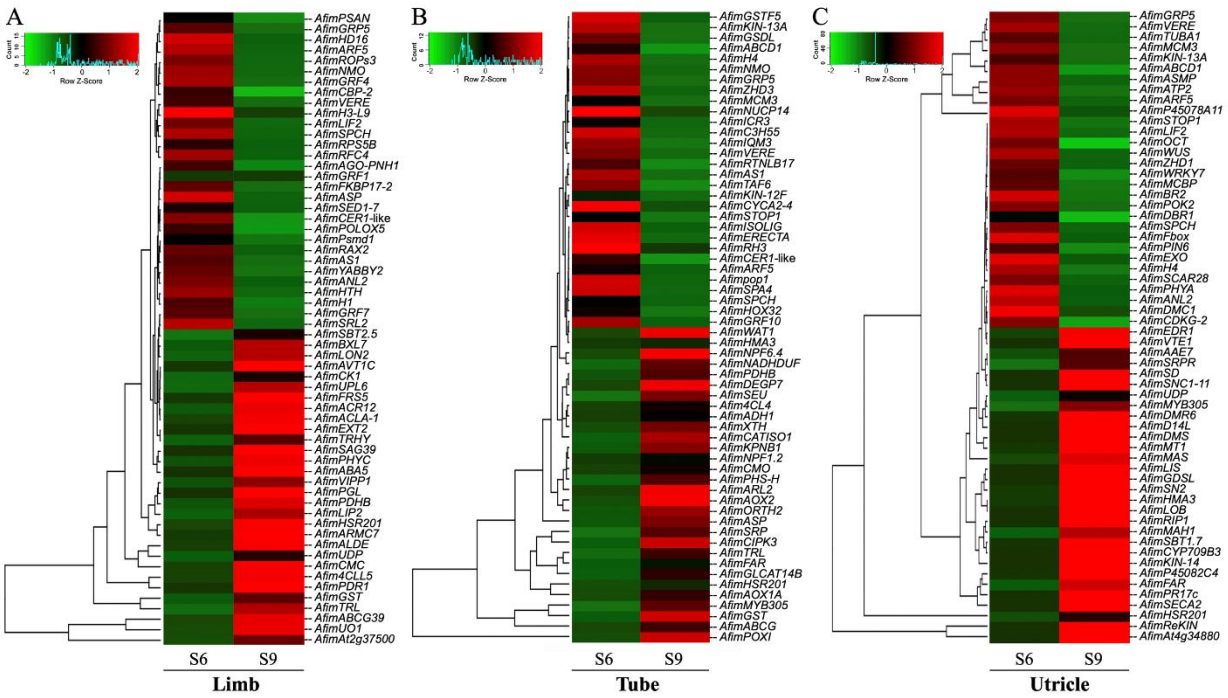

Figure 7. Hierarchical clustering heat maps of top 60 differentially expressed genes (DEGs) in the perianth of Aristolochia fimbriata. The genes are displayed in rows with normalized transcripts per million (TPMs) values for the comparisons Limb at S6 versus S9 developmental stage (A). Tube at S6 versus S9 stage (B). Utricle at S6 versus S9 (C). Each sample has three biological replicates. Gene expression levels are denoted at the top of the heatmap, with red and green indicating up-regulated and down-regulated expression, respectively.

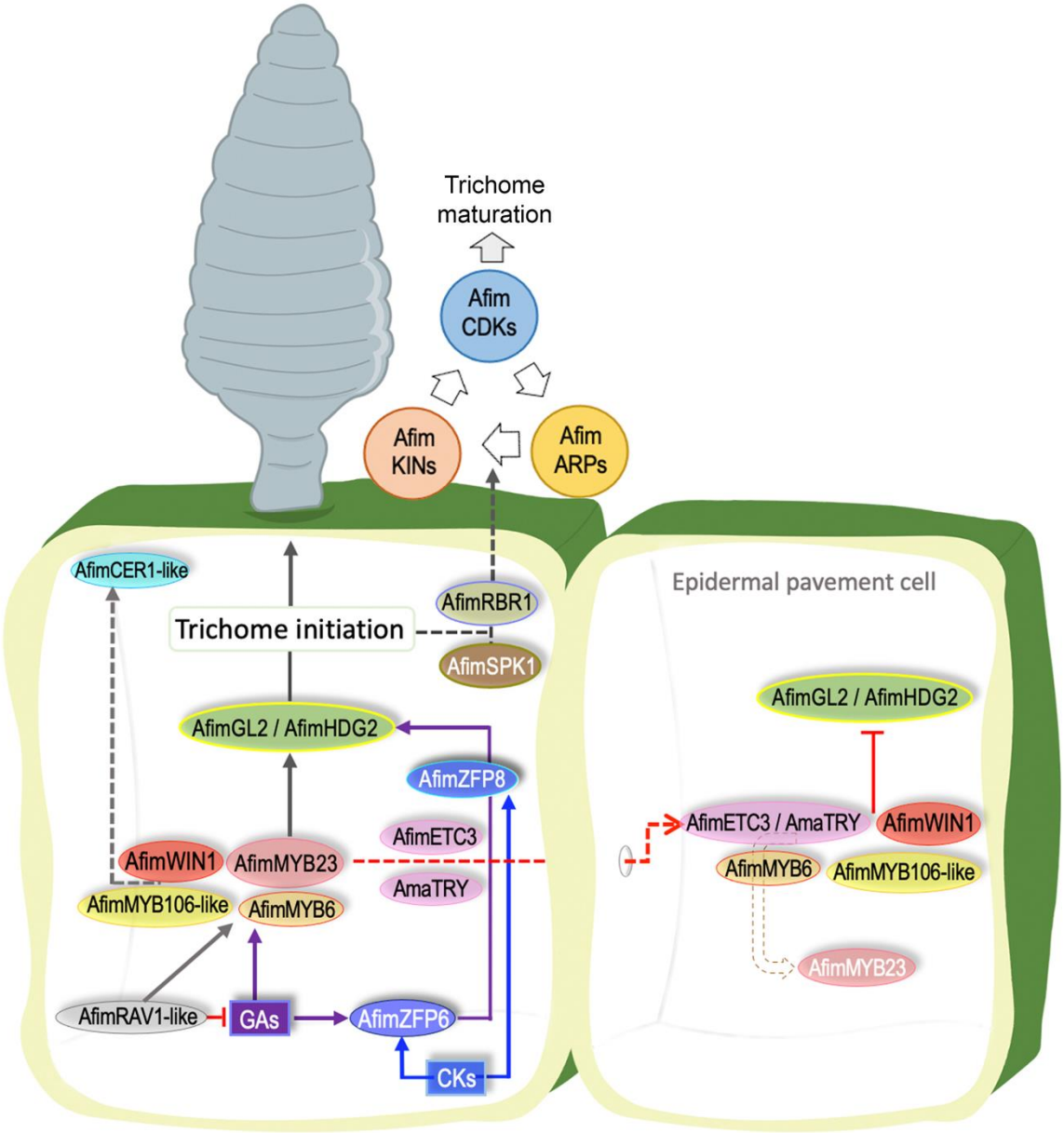

Figure 8. Hypothetical gene regulatory network (GRN) and hormone signaling underlying cell -fate and trichome development in the Aristolochia perianth. The putative activators of trichome initiation include AfimMYB23, AfimWIN1, and AfimMYB106-like. Then AfimGL2 or AfimHDG2 are activated, which in turn activates other transcription factors, such as AfimRAV-like might be also regulating an additional activation pathway of trichome development through the regulation of that trimeric complex. Negative regulation of trichome fate consists of the combined activity of AfimMYB6 and AfimETC3 (R3-MYB); AfimETC might be moving to the neighboring cells (red dash arrow). Gibberellins (GAs) and Cytokinins (CKs) contribute positively to the regulation of trichome development. GAs can stimulate the transcription of the ZINC FINGER PROTEIN 6 (AfimZFP6) gene, and then AfimZFP6 might be inducing the expression of AfimZFP8, and AfimZFP8 may control AfimGL2/AfimHDG2. AfimSPK1 might be controlling AfimRBR1 and then modulating different pathways of trichome maturation by controlling different genes related to cell cycle progression, cell polarity, and cytoskeleton dynamics (i. e.: AfimCDKs, AfimKINs, and AfimARPs).